THE EUROPEAN
PHYSICAL JOURNAL C

New Physics in $b \to s\ell^+\ell^-$ confronts new data on lepton universality

Marco Ciuchini[1,a], **António M. Coutinho**[2,b], **Marco Fedele**[3,c], **Enrico Franco**[4,d], **Ayan Paul**[5,6,e] ,
Luca Silvestrini[4,6,7,f], **Mauro Valli**[8,g]

[1] INFN, Sezione di Roma Tre, Via della Vasca Navale 84, 00146 Rome, Italy
[2] CFTP, Instituto Superior Técnico, Universidade de Lisboa, Avenida Rovisco Pais 1, 1049-001 Lisbon, Portugal
[3] Dept. de Física Quàntica i Astrofísica, Institut de Ciències del Cosmos (ICCUB), Universitat de Barcelona, Martí Franquès 1, 08028 Barcelona, Spain
[4] INFN, Sezione di Roma, P.le A. Moro 2, 00185 Rome, Italy
[5] DESY, Notkestraße 85, 22607 Hamburg, Germany
[6] Institut für Physik, Humboldt-Universität zu Berlin, 12489 Berlin, Germany
[7] Theoretical Physics Department, CERN, Geneva, Switzerland
[8] Department of Physics and Astronomy, University of California, Irvine, CA 92697-4575, USA

Abstract In light of the very recent updates on the R_K and R_{K^*} measurements from the LHCb and Belle collaborations, we systematically explore here imprints of New Physics in $b \to s\ell^+\ell^-$ transitions using the language of effective field theories. We focus on effects that violate Lepton Flavour Universality both in the Weak Effective Theory and in the Standard Model Effective Field Theory. In the Weak Effective Theory we find a preference for scenarios with the simultaneous presence of two operators, a left-handed quark current with vector muon coupling and a right-handed quark current with axial muon coupling, irrespective of the treatment of hadronic uncertainties. In the Standard Model Effective Field Theory we select different scenarios according to the treatment of hadronic effects: while an aggressive estimate of hadronic uncertainties points to the simultaneous presence of two operators, one with left-handed quark and muon couplings and one with left-handed quark and right-handed muon couplings, a more conservative treatment of hadronic matrix elements leaves room for a broader set of scenarios, including the one involving only the purely left-handed operator with muon coupling.

a e-mail: marco.ciuchini@roma3.infn.it

b e-mail: antonio.coutinho@roma3.infn.it

c e-mail: marco.fedele@icc.ub.edu

d e-mail: enrico.franco@roma1.infn.it

e e-mail: ayan.paul@desy.de

f e-mail: luca.silvestrini@roma1.infn.it

g e-mail: mvalli@uci.edu

1 Introduction

The past few years have brought us a thriving debate on the possible hints of New Physics (NP) from measurements of semileptonic B decays. In particular, Flavour Changing Neutral Current (FCNC) decay modes into multi-body final states, e.g. $B \to K^{(*)}\ell^+\ell^-$ and $B_s \to \phi\,\ell^+\ell^-$, bring forth a large number of experimental handles, see e.g. [1], that are extremely useful for NP investigations while also allowing to probe the Standard Model (SM) itself in detail [2–6]. The inference of what pattern is being revealed by the experimental observations is the crux of the debate.

Two distinct classes of observables characterize these semileptonic decays. The first is the class of angular observables arising from the kinematic distribution of the differential decay widths that have been measured at LHCb [7–13], Belle [14], ATLAS [15] and CMS [16–18]. These observables, mostly related to the muonic decay channel, while being sensitive to NP [6,19–22] are besieged by hadronic uncertainties [23–28]. The latter, associated with QCD long-distance effects – hard to estimate from first principles [29,30] – can saturate the measurements so as to be interpreted as possibly arising from the SM or can obfuscate the gleaning of NP from SM contributions [31–33]. Therefore, in the absence of a complete and reliable calculation of the hadronic long-distance contributions, a clear resolution of this debate based solely on the present set of angular measurements is hard to achieve. Improved experimental information in the near future [34] concerning, in particular, the electron modes is a subject of current cross-talk between the

theoretical and experimental communities [35,36], and may shed new light on this matter [37–39]. The second class of observables then becomes crucial to this debate. These are the Lepton Flavour Universality Violating (LFUV) ratios that hold the potential to conclusively disentangle NP contributions from SM hadronic effects. The latter are indeed lepton flavour universal [2,40]. Several hints in favour of LFUV have surfaced in the past few years in experimental searches at LHCb [41,42] and Belle [14]. These have led to a plethora of theoretical investigations [43–161], all oriented towards physics Beyond the Standard Model (BSM) able to accommodate such LFUV signals, mainly involving Z' or leptoquark mediators at scales typically larger than a few TeV and with some peculiar flavour structure needed to avoid clashing with the stringent bounds from meson–antimeson mixing and from other observables. Despite possible model-building challenges, the primary message here is clear: a statistically significant measurement of LFUV effects in FCNCs such as $b \rightarrow s\ell^+\ell^-$ decays would herald the discovery of NP unambiguously [162–167].

In this work we focus on the progress of this debate with the new measurements of R_K and R_{K^*} recently presented by the LHCb [168] and Belle collaborations [169]:

$$R_K [1.1, 6] \equiv \frac{Br\left(B^+ \rightarrow K^+\mu^+\mu^-\right)}{Br\left(B^+ \rightarrow K^+e^+e^-\right)}$$
$$= 0.846^{+0.060+0.016}_{-0.054-0.014} \text{ (LHCb)}, \qquad (1)$$

$$R_{K^*} [0.045, 1.1] \equiv \frac{Br\left(B \rightarrow K^*\mu^+\mu^-\right)}{Br\left(B \rightarrow K^*e^+e^-\right)}$$
$$= 0.52^{+0.36}_{-0.26} \pm 0.05 \text{ (Belle)}, \qquad (2)$$

$$R_{K^*} [1.1, 6] = 0.96^{+0.45}_{-0.29} \pm 0.11 \text{ (Belle)}. \qquad (3)$$

The LHCb result combines the re-analysis of the 2014 measurement together with more recent data, partially including the experimental information from Run II, and covers an invariant dilepton mass q^2 ranging in [1.1,6] GeV^2. The preliminary Belle measurement also covers larger values of the dilepton invariant mass, which however are not used in our analysis, as detailed below. While the central value of the measurement in Eq. (1) shifts towards the SM prediction [2,40], the statistical significance of the corresponding R_K *anomaly* remains interesting, at the level of 2.5σ. On the other hand, the result in Eq. (3) slightly weakens the significance of the R_{K^*} anomaly in this range of dilepton invariant mass.

In an attempt to better disentangle SM hadronic uncertainties and to zoom in on the importance of NP contributions, here we present a state-of-the-art analysis of $b \rightarrow s\ell^+\ell^-$ transitions where:

– We revisit our approach to QCD power corrections streamlined for efficiently capturing long-distance effects, which are of utmost relevance in the interpretation of the current experimental information on the $B \rightarrow K^*\mu^+\mu^-$ channel. We discuss several novelties about our new parameterization of hadronic contributions, recently introduced in [39];

– We make use of two distinct Effective Field Theory (EFT) frameworks, namely the $\Delta B = 1$ Weak Effective Hamiltonian and the Standard Model Effective Field Theory (SMEFT). The former EFT allows us to obtain a better insight on the dynamics at the decay scale, while the latter can offer a deeper link with BSM interpretations.

We review our theoretical framework in Sect. 2, where we also present a fresh look at the anatomy of R_K in light of the new LHCb measurement. We then provide a thorough description of our analysis procedure in Sect. 3. Finally, we collect and discuss all our main results in Sect. 4, supported also by Appendix A and Appendix B. We present our conclusions in Sect. 5.

2 Theoretical framework

As an introduction to the basic ingredients of our analysis we start by reviewing the standard EFT for $\Delta B = 1$ transitions, highlighting the distinction between short-distance and hadronic contributions. We then move on to LFUV effects in terms of SM gauge-invariant dimension-six operators, completing the EFT dictionary useful for understanding the results we present in Sect. 4.

2.1 Short distance vs long distance

The anatomy of $B \rightarrow K^{(*)}\ell^+\ell^-$, $B \rightarrow K^*\gamma$, $B_s \rightarrow \phi\ell^+\ell^-$ and $B_s \rightarrow \phi\gamma$ decays can be inspected with an effective field theory of weak interactions for $\Delta B = 1$ processes [170,171]. The corresponding effective Hamiltonian at the scale $\mu_b \sim m_b$ can be split in two parts:

$$\mathcal{H}^{\Delta B=1}_{\text{eff}} = \mathcal{H}^{\text{had}}_{\text{eff}} + \mathcal{H}^{\text{sl}+\gamma}_{\text{eff}}, \qquad (4)$$

where the first "hadronic" term contains only nonleptonic operators:

$$\mathcal{H}^{\text{had}}_{\text{eff}} = \frac{4G_F}{\sqrt{2}} \sum_{p=u,c} \lambda_p \left[C_1 Q_1^p + C_2 Q_2^p \right.$$
$$\left. + \sum_{i=3,\ldots,6} C_i P_i + C_8 Q_{8g} \right], \qquad (5)$$

involving the following set of relevant operators up to dimension six:

$$
\begin{aligned}
Q_1^p &= (\bar{s}_L \gamma_\mu T^a p_L)(\bar{p}_L \gamma^\mu T^a b_L), \\
Q_2^p &= (\bar{s}_L \gamma_\mu p_L)(\bar{p}_L \gamma^\mu b_L), \\
P_3 &= (\bar{s}_L \gamma_\mu b_L) \sum_q (\bar{q} \gamma^\mu q), \\
P_4 &= (\bar{s}_L \gamma_\mu T^a b_L) \sum_q (\bar{q} \gamma^\mu T^a q), \\
P_5 &= (\bar{s}_L \gamma_{\mu 1} \gamma_{\mu 2} \gamma_{\mu 3} b_L) \sum_q (\bar{q} \gamma^{\mu 1} \gamma^{\mu 2} \gamma^{\mu 3} q), \\
P_6 &= (\bar{s}_L \gamma_{\mu 1} \gamma_{\mu 2} \gamma_{\mu 3} T^a b_L) \sum_q (\bar{q} \gamma^{\mu 1} \gamma^{\mu 2} \gamma^{\mu 3} T^a q), \\
Q_{8g} &= \sqrt{\frac{\alpha_s}{64\pi^3}} \, m_b \bar{s}_L \sigma_{\mu\nu} G^{\mu\nu} b_R.
\end{aligned}
\tag{6}
$$

The second term features four-fermion operators constructed with leptonic and quark bilinears, together with the electromagnetic dipole operators,

$$
\mathcal{H}_{\text{eff}}^{\text{sl}+\gamma} = -\frac{4 G_F}{\sqrt{2}} \lambda_t \Bigg[C_7^{(\prime)} Q_{7\gamma}^{(\prime)} + C_9^{(\prime)} Q_{9V}^{(\prime)} + C_{10}^{(\prime)} Q_{10A}^{(\prime)} \\
+ C_S^{(\prime)} Q_S^{(\prime)} + C_P^{(\prime)} Q_P^{(\prime)} \Bigg],
\tag{7}
$$

including, up to dimension six, the operators:

$$
\begin{aligned}
Q_{7\gamma} &= \sqrt{\frac{\alpha_e}{64\pi^3}} \, m_b \bar{s}_L \sigma_{\mu\nu} F^{\mu\nu} b_R, \\
Q_{9V} &= \frac{\alpha_e}{4\pi} (\bar{s}_L \gamma_\mu b_L)(\bar{\ell} \gamma^\mu \ell), \\
Q_{10A} &= \frac{\alpha_e}{4\pi} (\bar{s}_L \gamma_\mu b_L)(\bar{\ell} \gamma^\mu \gamma^5 \ell), \\
Q_S &= \frac{\alpha_e}{4\pi} (\bar{s}_L b_R)(\bar{\ell} \ell), \\
Q_P &= \frac{\alpha_e}{4\pi} (\bar{s}_L b_R)(\bar{\ell} \gamma^5 \ell).
\end{aligned}
\tag{8}
$$

Note that in Eq. (8) we have omitted tensorial semileptonic structures under the reasonable assumption that NP exhibits a mass gap above the electroweak (EW) scale [43]. We have also omitted other hadronic operators that may arise beyond the SM, since we are focusing on LFUV. The primed operators Q_i' are obtained from Eq. (8) substituting $P_{R,L} \to P_{L,R}$ in the corresponding quark bilinears. Throughout the paper, CKM factors are defined as $\lambda_i = V_{is} V_{ib}^* = V_{i2} V_{i3}^*$, with $i = \{u, c, t\} = \{1, 2, 3\}$.

The short-distance physics in Eqs. (4)–(8) is, in general, captured by the Wilson coefficients (WCs), denoted as effective couplings $C^{(\prime)}$. Within the SM, at the dimension-six level, semileptonic chirality-flipped and (pseudo)scalar operators can be neglected, however they are potentially relevant for the study of NP effects. In our analysis, we evaluate SM WCs at the scale $\mu_b = 4.8$ GeV using state-of-the-art QCD and QED perturbative corrections, both in the matching [172–174] and

in the anomalous dimension of the operators involved [174–177].[1] We note that the remaining theoretical uncertainty on the SM WCs, at the level of few percent, can be neglected in this work.

In the absence of a unique UV complete model that can potentially be responsible for the measured hints of anomalies in the $b \to s$ transitions, the formalism of the effective Hamiltonian is extremely powerful. It allows to study the effects of BSM physics in a model-independent manner, where the presence of NP effects manifests itself as (lepton-flavour dependent) shifts of the WCs with respect to the SM values.[2] On the basis of previous global analyses which allow for LFUV effects [162–167,179–183], in this paper we allow for NP effects in the WCs of the operators $Q_{9,10,S,P}^{(\prime)\,\ell=e,\mu}$. We do not consider the case of NP effects in dipole operator coefficients $C_7^{(\prime)}$, since such a possibility is severely constrained by the inclusive radiative branching fraction of $B \to X_s \gamma$ among other measurements [184] and it is anyway irrelevant for LFUV. Moreover, in the following we also set aside the possibility of NP effects entering in Eq. (5), a case considered in the study by the authors of [73]. Our choice is, once more, primarily driven by our focus on LFUV effects. On more general grounds, one should stress that decoding LFU-conserving NP effects in current $b \to s$ data – a possibility recently considered in [185] – may be a challenging task [186], especially in light of unknown hadronic contributions.

Let us consider the $\bar{B} \to \bar{K}^* \ell^+ \ell^-$ transition as an example for setting up our notation. From the Hamiltonian defined in Eq. (4), it is possible to write down seven independent helicity amplitudes that, in full generality, describe a (pseudo)scalar particle decaying into a vector state and a dilepton pair. These helicity amplitudes can be combined together to define the decay branching ratio and the largest independent set of angular observables. In the basis defined in [29], these structures within the SM can be schematically written as[3]:

$$
\begin{aligned}
H_V^\lambda &\propto \left\{ C_9^{\text{SM}} \widetilde{V}_{L\lambda} + \frac{m_B^2}{q^2} \left[\frac{2 m_b}{m_B} C_7^{\text{SM}} \widetilde{T}_{L\lambda} - 16\pi^2 h_\lambda \right] \right\}, \\
H_A^\lambda &\propto C_{10}^{\text{SM}} \widetilde{V}_{L\lambda}, \quad H_P \propto \frac{m_\ell m_b}{q^2} C_{10}^{\text{SM}} \left(\widetilde{S}_L - \frac{m_s}{m_b} \widetilde{S}_R \right),
\end{aligned}
\tag{9}
$$

---

[1] The scale μ_b is here set by the scale at which form factors have been computed [178].

[2] In the present work, while we treat the SM short distance with all available quantum corrections included, for the NP WCs we neglect the running induced by gauge couplings. Consequently, they stay constant from the scale they have been generated, with the notable exception of the SMEFT contributions arsing only at one-loop via RGE, see Sect. 2.2 and Appendix B.

[3] Here we do not include the negligible contributions to $C_{S,P}^{(\prime)}$ from the SM for clarity.

with $\lambda = 0, \pm$. The factorizable part of these amplitudes, i.e. the one involving matrix elements of semileptonic local operators, is described by means of seven independent form factors, $\widetilde{V}_{0,\pm}$, $\widetilde{T}_{0,\pm}$ and $\widetilde{S}$ which are smooth functions of q^2. In Eq. (9) these are defined following the convention described in Appendix A of Ref. [31]. In addition to form factors, at first order in α_e, non-local contributions arise from the insertion of a quark current with each of the operators appearing in Eq. (5) [23,29]. As a result, non-factorizable QCD power corrections appear in H_V^λ according to the hadronic correlator [30,31, 181,187]:

$$h_\lambda(q^2) = \frac{\epsilon_\mu^*(\lambda)}{m_B^2} \int d^4x \; e^{iqx} \langle \bar{K}^* | T\{j_{em}^\mu(x) \mathcal{H}_{eff}^{had}(0)\} | \bar{B} \rangle .$$

$$(10)$$

For the factorizable part, in the large-recoil region (i.e. low dilepton invariant mass q^2) two light-cone sum rule (LCSR) computations are currently available [178,188]. These results are in reasonable agreement with the extrapolation of the form factors computed in lattice QCD at low recoil [189]. The information on the same form factors is enriched by a correlation matrix that keeps track also of heavy-quark symmetry relations as discussed in section 2.2 of Ref. [178].

On the contrary, the theoretical estimate of non-factorizable terms – denoted here generically by h_λ – is not so well under control. For the processes of interest, the largest contribution arises from current–current operators involving charm quarks, specifically Q_2^c [23,24], not parametrically suppressed by CKM factors or small WCs. This charm-loop effect stemming out of Eq. (10) is therefore a genuine long-distance contribution: it implies potentially sizable non-perturbative effects involving the charm quark pair with strong phases that are very difficult to estimate. While at low q^2 hard-gluon exchanges in the charm-loop amplitude can be addressed in the framework of QCD factorization (QCDF) [190], the evaluation of soft-gluon exchange effects remains, in this context, the toughest theoretical task [191]. A detailed analysis of soft-gluon exchanges in $B \to K$ transitions has been performed in Ref. [24]. There these contributions turned out to be sub-dominant in comparison with the QCDF estimate of the hard-gluon contributions, supporting previous results presented in [23].

For $B \to K^*$, the only estimate of h_λ currently available is the one carried out in Ref. [23] using LCSR techniques in the single soft-gluon approximation, valid for $q^2 \ll 4m_c^2$. The regime of validity of the result is then extended to the whole large-recoil region by means of a phenomenological model based on dispersion relations. While an estimate of the error budget is attempted in Ref. [23], there are potentially large systematic effects, related for instance to the lack of control over strong phases, that are difficult to quantify reliably, in particular when approaching the $c\bar{c}$ threshold at

$q^2 \sim 4m_c^2$ [31], close to the J/ψ resonance where quark–hadron duality is questionable even in the heavy quark limit [192]. Note that the same considerations also apply to the case of $B_s \to \phi \ell^+ \ell^-$, for which a similar LCSR evaluation of the charm-loop effect is still pending, leaving room also for appreciable $SU(3)_F$ breaking effects [26].

Recently, renewed attempts to obtain a better grasp of the non-factorizable terms have appeared in the literature [27,28]. Both works turn out to be in agreement with the results from Ref. [23]. However, in Ref. [27] – where h_λ is assumed to be well-described as a sum of relativistic Breit-Wigner functions – the authors found a very similar result to the one in [23] only in the case of vanishing strong phases, while quite different outcomes may be obtained for different assumptions on the same phases. In turn, the authors of Ref. [28] exploited the analytic properties of the amplitudes in order to perform a conformal expansion of h_λ, isolating physical poles and ensuring unitarity. They use resonant data and additional theoretical information at negative q^2 to fix the coefficients of the expansion, including estimates of strong phases due to the presence of a second branch cut in the amplitude (generated for instance by intermediate states with two charmed mesons), which represents a challenge for the formalism as well as for the numerical estimate. Despite the quite good agreement with the numerical result presented in [23], the coefficients obtained in [28] for the z-expansion of h_λ point to a poor convergence of the series, casting doubts on the actual q^2 shape of the h_λ functions if more terms were to be included in the expansion.

In this work, we are therefore well-motivated to consider the available LCSR estimates on h_λ from Ref. [23] with a certain degree of caution. To this end, we have already proposed in Refs. [31,32,166] a phenomenological expansion of h_λ in powers of q^2 in the large-recoil region, inspired by Ref. [30]. We use $B \to K^* \mu^+ \mu^-$ and $B \to K^* \gamma$ measurements in order to constrain the coefficients of the expansion, and enforce the results from Ref. [23] under two different scenarios:

– A *phenomenological model driven* (PMD) approach, employing LCSR results extrapolated by means of dispersion relations in the whole low-q^2 region for the decay;
– A *phenomenological data driven* (PDD) approach, taking into account LCSR results only far from the $c\bar{c}$ threshold and exploiting the results in Ref. [23] for $q^2 = 0, 1$ GeV^2, with their phases and q^2 dependence inferred from experimental data.

It is important to note that the PDD approach entails a loss of constraining power in the NP analysis, as some of the hadronic coefficients can mimic LFU NP effects, and therefore should be considered as the most conservative approach

towards the assessment of NP effects. Eventually, we also highlight that – differently from what done in Ref. [193] – the extraction of the hadronic coefficients in the PDD approach relies essentially on the experimental information stemming from the same q^2 region where our phenomenological expansion is used. To better investigate the interplay between hadronic contributions and possible NP ones, in this work we use a recent improvement of our parameterization for h_λ with the expansion presented in [39]:

$$
\begin{aligned}
h_-(q^2) &= -\frac{m_b}{8\pi^2 m_B}\widetilde{T}_{L-}(q^2)h_-^{(0)} - \frac{\widetilde{V}_{L-}(q^2)}{16\pi^2 m_B^2}h_-^{(1)}q^2 \\
&\quad + h_-^{(2)}q^4 + \mathcal{O}(q^6)\,, \\
h_+(q^2) &= -\frac{m_b}{8\pi^2 m_B}\widetilde{T}_{L+}(q^2)h_-^{(0)} - \frac{\widetilde{V}_{L+}(q^2)}{16\pi^2 m_B^2}h_-^{(1)}q^2 \\
&\quad + h_+^{(0)} + h_+^{(1)}q^2 + h_+^{(2)}q^4 + \mathcal{O}(q^6)\,, \\
h_0(q^2) &= -\frac{m_b}{8\pi^2 m_B}\widetilde{T}_{L0}(q^2)h_-^{(0)} - \frac{\widetilde{V}_{L0}(q^2)}{16\pi^2 m_B^2}h_-^{(1)}q^2 \\
&\quad + h_0^{(0)}\sqrt{q^2} + h_0^{(1)}(q^2)^{\frac{3}{2}} + \mathcal{O}((q^2)^{\frac{5}{2}})\,.
\end{aligned}
\tag{11}
$$

This choice allows us to write the helicity amplitudes H_V^λ in Eq. (9) as

$$
\begin{aligned}
H_V^- &\propto \Bigg\{ \left(C_9^{\text{SM}} + h_-^{(1)}\right)\widetilde{V}_{L-} \\
&\quad + \frac{m_B^2}{q^2}\left[\frac{2m_b}{m_B}\left(C_7^{\text{SM}} + h_-^{(0)}\right)\widetilde{T}_{L-} - 16\pi^2 h_-^{(2)}q^4\right]\Bigg\}\,, \\
H_V^+ &\propto \Bigg\{ \left(C_9^{\text{SM}} + h_-^{(1)}\right)\widetilde{V}_{L+} + \frac{m_B^2}{q^2}\Bigg[\frac{2m_b}{m_B}\left(C_7^{\text{SM}} + h_-^{(0)}\right)\widetilde{T}_{L+} \\
&\quad - 16\pi^2\left(h_+^{(0)} + h_+^{(1)}q^2 + h_+^{(2)}q^4\right)\Bigg]\Bigg\}\,, \\
H_V^0 &\propto \Bigg\{ \left(C_9^{\text{SM}} + h_-^{(1)}\right)\widetilde{V}_{L0} + \frac{m_B^2}{q^2}\Bigg[\frac{2m_b}{m_B}\left(C_7^{\text{SM}} + h_-^{(0)}\right)\widetilde{T}_{L0} \\
&\quad - 16\pi^2\sqrt{q^2}\left(h_0^{(0)} + h_0^{(1)}q^2\right)\Bigg]\Bigg\}\,.
\end{aligned}
\tag{12}
$$

With this definition for the h_λ-coefficients, it is manifest that $h_-^{(0)}$ and $h_-^{(1)}$ can be considered as constant shifts to the WCs $C_{7,9}^{\text{SM}}$, hence indistinguishable from NP contributions to $Q_{7\gamma,9V}$. Consequently, it is not possible to extract $h_-^{(0)}$ and $h_-^{(1)}$ directly from data unless one assumes the absence of NP effects. On the other hand, it is also not possible to ascertain the presence of NP without a theory input for these hadronic effects. The advantage of the parameterization in Eqs. (11)–(12) becomes clear when any of the remaining h_λ-coefficients turns out to be non-vanishing, since they likely spot purely

hadronic contributions.[4] In Sect. 3 we report the details of the implementation of our PMD and PDD approaches for non-factorizable contributions in the present numerical analysis.

2.2 The SMEFT perspective

Previous model-independent analyses of $b \rightarrow s\ell^+\ell^-$ anomalies have essentially pointed to $\mathcal{O}(10\,\text{TeV})$ NP for $\mathcal{O}(1)$ effective couplings in order to produce a $\sim 25\%$ shift of the SM WC values of the semileptonic operators $Q_{9V,10A}$. The UV dynamics underlying these NP effects is then expected to exhibit a reasonable mass gap with the SM theory. Hence, a quite natural choice for deeper BSM insights is the gauge-invariant framework of the SMEFT [194,195].

NP imprints in $b \rightarrow s$ transitions in the context of SM gauge-invariant operators have been extensively investigated in [43,53,196] and a systematic study of flavour physics constraints from $\Delta F = 2$ processes in the SMEFT has been recently performed in [197]. For $b \rightarrow s\ell^+\ell^-$ anomalies, a dedicated analysis with SMEFT operators was already carried out in Ref. [76]. In what follows we proceed along the lines outlined in these works.[5] The set of $SU(2)_L \times U(1)_Y$ invariant four-fermion operators in which we are mainly interested in this study reads:

$$
\begin{aligned}
O_{ijkl}^{LQ^{(1)}} &= (\bar{L}_i\gamma_\mu L_j)(\bar{Q}_k\gamma^\mu Q_l)\,, \\
O_{ijkl}^{LQ^{(3)}} &= (\bar{L}_i\gamma_\mu\tau^A L_j)(\bar{Q}_k\gamma^\mu\tau^A Q_l)\,, \\
O_{ijkl}^{Qe} &= (\bar{Q}_i\gamma_\mu Q_j)(\bar{e}_k\gamma^\mu e_l)\,, \\
O_{ijkl}^{Ld} &= (\bar{L}_i\gamma_\mu L_j)(\bar{d}_k\gamma^\mu d_l)\,, \\
O_{ijkl}^{ed} &= (\bar{e}_i\gamma_\mu e_j)(\bar{d}_k\gamma^\mu d_l)\,, \\
O_{ijkl}^{LedQ} &= (\bar{L}_i e_j)(\bar{d}_k Q_l)\,,
\end{aligned}
\tag{13}
$$

where $i, j, k, l = 1, 2, 3$ are generation indices, $\tau^{A=1,2,3}$ are Pauli matrices (a sum over A in the equations above is understood), weak doublets are in upper case and $SU(2)_L$ singlets are in lower case.

The operators appearing in Eq. (13) correspond to the set that matches at tree level on the semileptonic operators in Eq. (8) in an operator product expansion truncated at dimension six. The SMEFT tree-level matching is naturally performed at the scale $\mu_{\text{EW}} \sim \mathcal{O}(M_W)$. For BSM dynamics that distinguishes the leptonflavour $\ell = \{e, \mu, \tau\} = \{1, 2, 3\}$

---

[4] Note that this statement is accurate as long as NP effects do not feed any of the WCs in Eq. (5).

[5] We are not going to take into account the SMEFT contributions to the CKM parameters recently worked out in [198], since they cannot accommodate for LFUV effects.

in $b \to s$ transitions, the relations connecting the WCs of $Q^{(')}_{9,10,S,P}$ to the ones in the SMEFT-operator basis are:[6]

$$C^{\mathrm{NP}}_{9,\ell} = \mathcal{N}_\Lambda \left(C^{LQ^{(1)}}_{\ell\ell23} + C^{LQ^{(3)}}_{\ell\ell23} + C^{Qe}_{23\ell\ell} \right),$$

$$C^{\mathrm{NP}}_{10,\ell} = \mathcal{N}_\Lambda \left(C^{Qe}_{23\ell\ell} - C^{LQ^{(1)}}_{\ell\ell23} - C^{LQ^{(3)}}_{\ell\ell23} \right),$$

$$C'^{,\mathrm{NP}}_{9,\ell} = \mathcal{N}_\Lambda \left(C^{ed}_{\ell\ell23} + C^{Ld}_{\ell\ell23} \right),$$

$$C'^{,\mathrm{NP}}_{10,\ell} = \mathcal{N}_\Lambda \left(C^{ed}_{\ell\ell23} - C^{Ld}_{\ell\ell23} \right),$$

$$C^{\mathrm{NP}}_{S,\ell} = -C^{\mathrm{NP}}_{P,\ell} = \mathcal{N}_\Lambda C^{LedQ}_{\ell\ell23},$$

$$C'^{,\mathrm{NP}}_{S,\ell} = C'^{,\mathrm{NP}}_{P,\ell} = \mathcal{N}_\Lambda \left(C^{LedQ}_{\ell\ell32} \right)^*, \tag{14}$$

where we introduced the complex factor

$$\mathcal{N}_\Lambda \equiv (\pi v^2)/(\alpha_e \lambda_t \Lambda^2),$$

with $v^2/2 = \langle H^\dagger H \rangle$, H being the SM Higgs doublet. For a NP scale Λ of 30 TeV one has $|\mathcal{N}_\Lambda| \simeq 0.7$. Equation (14) is valid in the basis where charged lepton and down-type quark Yukawa couplings are diagonal. This choice simplifies the analysis by avoiding lepton flavour violation and constraints from quark flavour transitions other than $b \to s$.

Note that even under this assumption, the operators in Eq. (13) may be, in principle, testable in other interesting processes other than $b \to s\ell^+\ell^-$ transitions. The most notable opportunity may be offered by the channel $B \to K^{(*)}\nu\bar{\nu}$ [201], sensitive to the operators composed of weak doublets in both lepton and quark currents. At the present experimental sensitivity [202], this channel turns out to have a relatively mild interplay with $b \to s\ell^+\ell^-$ measurements [86,113]. Interestingly, with the advent of more data [34] one may hope to distinguish NP effects of $O^{LQ^{(3)}}$ from the ones of $O^{LQ^{(1)}}$ due to an accurately measured light-lepton LFUV ratio in semileptonic $b \to c$ transitions [54,86]. Still, for the purposes of our model-independent study, $O^{LQ^{(1,3)}}_{ii23}$, $i = \{1, 2\}$, are indistinguishable, as in Ref. [76]. Without loss of generality, the set of operators in Eq. (13) remains indeed the one primarily sensitive to the measurements considered in this work.

Going beyond Eq. (13), one may extend the discussion to the operators induced at one-loop level that are a genuine product of the renormalization group evolution (RGE) in the SMEFT [203,204]. Equipped with the aforementioned assumption on the SMEFT flavour structure, in the leading-log approximation and leading expansion in the top Yukawa

coupling y_t, the matching conditions induced by one-loop RGE read as:

$$C^{\mathrm{NP}}_{9,\ell} = \mathcal{N}_\Lambda \lambda_t \left(\frac{y_t}{4\pi} \right)^2 \log \left(\frac{\Lambda}{\mu_{\mathrm{EW}}} \right) \left(C^{HL^{(3)}}_{\ell\ell} - C^{HL^{(1)}}_{\ell\ell} \right.$$
$$\left. - C^{He}_{\ell\ell} + C^{Lu}_{\ell\ell33} + C^{eu}_{\ell\ell33} \right),$$

$$C^{\mathrm{NP}}_{10,\ell} = \mathcal{N}_\Lambda \lambda_t \left(\frac{y_t}{4\pi} \right)^2 \log \left(\frac{\Lambda}{\mu_{\mathrm{EW}}} \right) \left(C^{HL^{(1)}}_{\ell\ell} - C^{HL^{(3)}}_{\ell\ell} \right.$$
$$\left. - C^{He}_{\ell\ell} - C^{Lu}_{\ell\ell33} + C^{eu}_{\ell\ell33} \right), \tag{15}$$

where we have reported again only contributions that matter for the discussion of LFUV effects coming from dimension-six operators with Higgs doublet and lepton bilinears,

$$O^{HL^{(1)}}_{\ell\ell} = (H^\dagger i \overleftrightarrow{D}_\mu H)(\bar{L}_\ell \gamma^\mu L_\ell),$$

$$O^{HL^{(3)}}_{\ell\ell} = (H^\dagger i \overleftrightarrow{D}^A_\mu H)(\bar{L}_\ell \gamma^\mu \tau^A L_\ell),$$

$$O^{He}_{\ell\ell} = (H^\dagger i \overleftrightarrow{D}_\mu H)(\bar{e}_\ell \gamma^\mu e_\ell), \tag{16}$$

together with semileptonic operators involving a right-handed top-quark current,

$$O^{Lu}_{\ell\ell33} = (\bar{L}_\ell \gamma_\mu L_\ell)(\bar{u}_3 \gamma^\mu u_3),$$

$$O^{eu}_{\ell\ell33} = (\bar{e}_\ell \gamma_\mu e_\ell)(\bar{u}_3 \gamma^\mu u_3). \tag{17}$$

The expression in Eq. (15) needs to be added to the tree-level matching already given in Eq. (14). Next-to-leading order SMEFT matching conditions, invoked to reduce the matching-scale dependence on the overall result (and involving renormalization scheme-dependent finite parts of one-loop diagrams), have been computed in Refs. [196,205]. Within the leading-log approximation undertaken in this work, these corrections should be considered as sub-leading to the RGE-induced contributions given in Eq. (15). Obviously, the same $\sim 25\%$ shift of the SM WC $C_{9,10}$ needed for a qualitative explanation of $b \to s\ell^+\ell^-$ anomalies, if obtained through the RG mixing in Eq. (15), requires NP scales of $\mathcal{O}(\mathrm{TeV})$ for $\mathcal{O}(1)$ couplings. Therefore, in these particular scenarios the underlying BSM physics should be much closer to collider reach compared to cases in which the operators in Eq. (14) are directly generated by NP [95]. As already commented in Ref. [76], operators appearing in Eq. (16) are particularly well constrained by EW precision observables [199,200], making them irrelevant in the present context. Our analysis on SMEFT RGE-induced contributions will then focus only on the operators listed in Eq. (17) above. Note, however, that these operators can also be constrained at the loop level by EW data, see Refs. [131,206]. We dedicate our Appendix B to the inspection of this set of operators, where we highlight a non-trivial interplay between the assumption made on hadronic contributions in analysis of

---

[6] Dimension-six operators made of Higgs doublets and quark bilinears should also appear [43], but yield a lepton flavour universal contribution. They are severely constrained both by EW and Higgs data, see [199, 200], and by $\Delta F = 2$ measurements [197]. They will not be further considered here.

$b \to s\ell^+\ell^-$ data and the information coming from EW precision measurements relevant in this context [207].

2.3 New Physics effects in R_K

We wish to end this section reviewing the relevance of R_K for NP and its complementarity with other present and possibly forthcoming LFUV measurements, as R_{K^*} and R_ϕ. This completes the stage setup for the presentation and discussion of the results collected in Sect. 4.

The ratio reported in Eq. (1) can be reasonably approximated in terms of a simple phenomenological formula. Since the minimum q^2-value probed in the bin of interest is much greater than light lepton masses and it is far from the light-cone region, one may neglect effects proportional to m_ℓ^2 and the contribution coming from the electromagnetic dipole operator. Furthermore, one may also opt to neglect non-factorizable hadronic contributions present in $B \to K\ell^+\ell^-$, retaining them as sub-leading effects, possibly supported by the estimates illustrated in Ref. [24]. Then, up to percent level QED corrections discussed in Ref. [208], similarly to Refs. [76,162,163,167] we can express R_K in terms of NP WCs simply as:

$$R_K[1.1, 6]$$
$$\simeq \left\{ 1 + 0.23(C_{9,\mu}^{\mathrm{NP}} + C_{9,\mu}'^{,\mathrm{NP}}) - 0.25(C_{10,\mu}^{\mathrm{NP}} + C_{10,\mu}'^{,\mathrm{NP}}) \right.$$
$$+ 0.057(C_{9,\mu}^{\mathrm{NP}} C_{9,\mu}'^{,\mathrm{NP}} + C_{10,\mu}^{\mathrm{NP}} C_{10,\mu}'^{,\mathrm{NP}}) + 0.029\left[(C_{9,\mu}^{\mathrm{NP}})^2 \right.$$
$$\left. \left. + (C_{9,\mu}'^{,\mathrm{NP}})^2 + (C_{10,\mu}^{\mathrm{NP}})^2 + (C_{10,\mu}'^{,\mathrm{NP}})^2 \right] \right\} \Big/ \{1 + \mu \to e\}$$
$$(18)$$

or in terms of the WCs for the gauge-invariant combinations in Eq. (13):

$$R_K[1.1, 6]$$
$$\simeq \left\{ 1 + r_\Lambda \left[0.16(C_{2223}^{ed} + C_{2322}^{Qe}) - 5.1(C_{2223}^{Ld} + C_{2223}^{LQ}) \right. \right.$$
$$+ 13 r_\Lambda \left(C_{2223}^{ed} C_{2322}^{Qe} + C_{2223}^{Ld} C_{2223}^{LQ} \right)$$
$$+ 6.6 r_\Lambda \left((C_{2223}^{ed})^2 + (C_{2322}^{Qe})^2 + (C_{2223}^{Ld})^2 \right.$$
$$\left. \left. \left. + (C_{2223}^{LQ})^2 \right) \right] \right\} \Big/ \left\{ 1 + r_\Lambda [22 \to 11] \right\},$$
$$(19)$$

where in the last expression $C_{\ell\ell23}^{LQ} \equiv C_{\ell\ell23}^{LQ^{(1)}} + C_{\ell\ell23}^{LQ^{(3)}}$, $r_\Lambda \equiv 10^3 (v/\Lambda)^2$ and λ_t is approximated as real. In both Eqs. (18) and (19), we assume real NP coefficients. Notice that, in the cases at hand, quadratic terms are suppressed as $(\frac{\pi}{\alpha_e} \frac{v^2}{\Lambda^2})^2$, while linear terms with dimension-eight operators are suppressed as $\frac{\pi}{\alpha_e} \frac{v^4}{\Lambda^4}$. Therefore, we can meaningfully retain the quadratic terms. Moreover, we have neglected the NP contribution of (pseudo)scalar operators: while being

constrained by $B \to \ell^+\ell^-$ measurements, these operators cannot address at the same time other $b \to s\ell^+\ell^-$ anomalies as the one(s) related to R_{K^*}.[7] Finally, note that if one would like to consider also tensor structures [44], a combined explanation of R_K and R_{K^*} would not be possible [94], and embedding in UV models would be challenging [3,43].

In Fig. 1 we show the impact on R_K in the bin discussed so far of each of the operators considered here in the WET (left panel), see Eq. (18), and in the SMEFT (right panel), see Eq. (19). The range on the x-axis in Fig. 1 covers $\mathcal{O}(1)$ effects relative to the short-distance SM contributions. The SM limit is emphasized by the silver dot-dashed lines, and the new R_K measurement is represented by the horizontal orange band, drawn according to experimental central value and standard deviation, see Eq. (1).

It is clear from what is depicted for the WET that operators featuring both left-handed and right-handed $b \to s$ currents are eligible for a satisfactory explanation of the measured value of R_K. In particular, one cannot distinguish effective couplings related to left-handed or right-handed $b \to s$ currents within operators that have the same leptonic structure, since they constructively interfere in Eq. (18). Moreover, as highlighted in the plot, the NP contribution required to explain the present R_K measurement is now about one fifth of the SM one. Therefore, the linearized limit of Eq. (18) may be a good approximation in order to appreciate how LFUV effects actually probe the $\mu - e$ combination of the leptonic current. This fact is captured in the plot by the mirror-like behaviour of red-blue and magenta-cyan line pairs with respect to the SM limit. In the same panel, axial and vectorial leptonic effective couplings turn out also to be mirror-like as a reflection of the SM result: $C_9^{\mathrm{SM}} \sim -C_{10}^{\mathrm{SM}}$.

Similar considerations apply to the case of SMEFT operators with leptonic weak doublets, requiring only about 15% of the SM WC value for $Q_{9V,10A}$ to accommodate R_K within a NP scale of $\Lambda = 30$ TeV, yielding $|C_{\ell\ell23}^{LQ,Ld}| \sim 0.8$. However, the correlations induced by the $SU(2)_L \times U(1)_Y$ gauge symmetry no longer allow a full set of 8 different viable solutions for the R_K anomaly. From the right panel of Fig. 1, NP effects from SMEFT operators featuring exclusively right-handed muonic currents are ruled out, while the electronic counterparts are still available at the expense of larger NP effects, $\gtrsim 35\%$ of the SM short-distance physics for the same $\Lambda = 30$ TeV. Interestingly, among the RGE-induced set of operators reported in Eq. (17) we can then exclude O_{2233}^{eu}.

The bottom line drawn from Fig. 1 refers merely to the inspection of one single operator at a time contributing to R_K. However, in the broader picture offered by the whole set of available $b \to s\ell^+\ell^-$ measurements, we may end up with observable quantities that provide information on

---

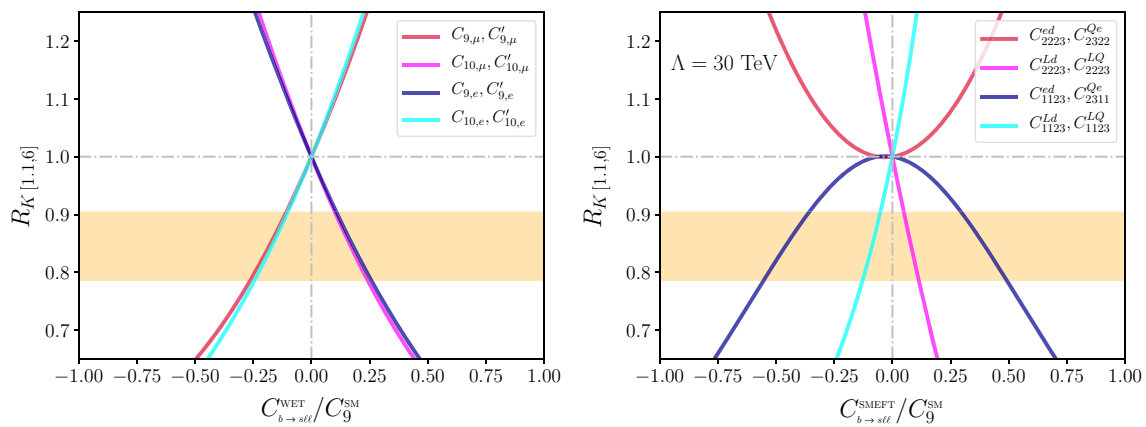[7] Within the SMEFT, they cannot simultaneously explain the R_K anomaly as well.

Fig. 1 The impact on R_K of each of the NP operators in the two EFT frameworks considered. The orange band highlights the new R_K measurement, while the dashed-dot silver lines mark the SM value. In both panels the range on the x-axis covers up to $\mathcal{O}(1)$ effects with respect to SM short distance relatively to the low-energy scale $\mu_b \sim m_b$. SMEFT contributions are assumed to be generated at the NP scale of 30 TeV

NP orthogonal to what outlined from the R_K anatomy. Of particular significance, the LFUV ratio R_{K^*} has been originally recognized in Ref. [47] to be a complementary probe of NP with respect to R_K. Indeed, while being very sensitive to BSM physics, in the limit where the longitudinal polarization fraction in the $B \to K^* \ell^+ \ell^-$ channel were exactly equal to unity, R_{K^*} would be fully sensitive to destructive interference between left-handed and right-handed $b \to s$ effective couplings, and hence complementary to what is depicted in Eq. (18) for R_K. In the same spirit of Ref. [167], one may then look at the ratio of measured LFUV ratios, i.e. the R_{K^*} experimental value in the bin [1.1,6] GeV^2 from [42,169] over the new measurement of R_K from [168],

$$R_{K^*}[1.1, 6]/R_K[1.1, 6] \simeq 0.86 \pm 0.13, \tag{20}$$

discovering a hint for non-zero effective couplings for the operators $Q'_{9V,10A}$, part of Eq. (7). Moreover, going beyond LFUV observables, one may supplement the information of Eq. (20) with the measurements of $B \to K^{(*)} \mu^+ \mu^-$ branching fractions and, most importantly, with the related angular analyses. In particular, with the inclusion of the angular observable P'_5 – particularly sensitive to NP effects in the operator Q_{9V} [180,209] – one may end up concluding that the new experimental value of R_K currently points to effects in both left-handed and right-handed $b \to s$ currents of dimension-six operators built up with the muonic vectorial current. As such, previously claimed minimal solutions for $b \to s \ell^+ \ell^-$ anomalies – involving only Q_{9V} or O^{LQ} – would now seem to be more disfavoured in view of the need for NP effects also in right-handed currents.

Unfortunately, the above qualitative considerations remain subject to several uncertainties. First of all, the longitudinal polarization fraction of $B \to K^* \ell^+ \ell^-$ in the bin of interest is not equal to unity [210]: this fact already makes the R_{K^*} observable less orthogonal to R_K in the study of NP [163].

Moreover, longitudinal and transverse polarization fractions are sensitive to $\Lambda_{\rm QCD}/m_b$ power corrections not fully under control [47,163]. This also suggests an experimental information that would be important to handle in the future: the measurement of $R_{K^*}^{\rm T,L}[1.1, 6]$, i.e. the ratio of longitudinal and transverse parts of the $B \to K^* \ell^+ \ell^-$ amplitude in the q^2-bin [1.1,6] GeV^2. These quantities would be less sensitive to unknown hadronic effects, and distinctively sensitive to NP effects in $C_{9,10} \pm C'_{9,10}$ combinations [163,166]. Similar information could be extracted from $B_s \to \phi \ell^+ \ell^-$ as well.

Secondly, as already noted at the beginning of Sect. 2, the same angular observables measured in $B \to K^* \mu^+ \mu^-$ are also affected by non-factorizable QCD effects. Only corresponding LFUV combinations as the one proposed in Ref. [35,36] and recently reanalyzed in [186] may help to disentangle genuine NP effects from hadronic contributions theoretically not well-understood. At present, the only available measurement of this sort is given by Belle [14] and it is (unfortunately) of limited statistical significance, but more will certainly come in the next years [34].

In the end, a careful study of $b \to s \ell^+ \ell^-$ anomalies calls for a global analysis that can go well beyond the qualitative picture highlighted above, taking care of all the aforementioned subtleties in a framework where a non-trivial interplay between genuine NP effects and hadronic contributions is allowed. The analysis performed in this study, presented in Sect. 4, is precisely dedicated to make interpretations of the underlying NP scenarios behind current $b \to s \ell^+ \ell^-$ anomalies as robust as possible.

3 Experimental and theoretical input

In this section we plan to review the baseline of our analysis, the experimental dataset included, and the assumptions

made throughout this work. In the present study we perform a global analysis on a comprehensive set of $b \rightarrow s\ell^+\ell^-$ data with state-of-the-art theoretical computations, within a Bayesian framework.

We adopt for this matter the public HEPfit package [211], whose Markov Chain Monte Carlo (MCMC) analysis framework employs the Bayesian Analysis Toolkit (BAT) [212]. In our MCMC analysis we vary from a minimum of 60 to a maximum of 80 parameters on a case by case basis. Within the Metropolis-Hastings algorithm implemented in BAT, we set up, for the scenarios presented in Sect. 4, MCMC runs involving 240 chains with a total of 2.4 million events per run, collected after an equivalent number of pre-run iterations.

We perform a Bayesian model comparison between different scenarios evaluating for each of them an *Information Criterion* (IC). This quantity offers an approximation of the predictive accuracy of the model [213], and it is characterized by the mean and the variance of the posterior probability density function (*p.d.f.*) of the log-likelihood $\log \mathcal{L}$, see Ref. [214],

$$IC \equiv -2\overline{\log \mathcal{L}} + 4\sigma^2_{\log \mathcal{L}}, \tag{21}$$

where the first term gives an estimate of the predictive accuracy (actually, an overestimate since the same data have already been used in the fit), and the second term corrects for the overestimate by adding a penalty factor which counts the effective number of fitted parameters. Model selection between two scenarios proceeds according to the smallest IC value reported and the extent to which a model should be preferred over another one follows the canonical scale of evidence of Ref. [215], related in this context to (positive) IC differences. In the following Sect. 4, for convenience we are going to present a discussion based on $\Delta IC \equiv IC_{SM} - IC_{NP}$.[8] In particular, we quote in Tables 1 and 2 for each NP scenario the ΔIC value. We wish to stress that a larger value of ΔIC corresponds to a better improvement of the model compared to the SM.

Regarding the experimental dataset considered in this study, we include all the most recent measurements related to $b \rightarrow s\ell^+\ell^-$ transitions that can have a valuable impact in our global fit. We briefly list them below with some additional comments:

---

[8] It is interesting to perform a SM global fit in order to have reference values for the *IC* to compare with. The fits yield an *IC* of 193 for the PDD approach, and 215 for the PMD one. Recalling that models with smaller values for the *IC* are preferred, the PDD approach provides a better SM fit compared to the PMD one, since anomalies in the angular analysis of $B \rightarrow K^* \mu^+ \mu^-$ can be accommodated through larger long-distance contributions, see Ref. [31].

Table 1 Values of the WET WCs fit from data in all the considered scenarios along with relative ΔIC. The italic values highlight the PMD results when this approach can be used to address the experimental data in a particular scenario. The PDD results are presented for all cases. For the definition of the two approaches, see Sect. 2.1

	Mean (rms)	ΔIC
$C_{9,\mu}^{\mathrm{NP}}$	$-1.20(27)$	14
	$-1.21(16)$	*50*
$C_{10,e}^{\mathrm{NP}}$	$-0.87(24)$	15
$(C_{9,\mu}^{\mathrm{NP}}, C_{9,e}^{\mathrm{NP}})$	$(-1.61(48), -0.56(53))$	13
	$(-1.28(18), -0.27(34))$	*48*
$(C_{9,\mu}^{\mathrm{NP}}, C_{9,\mu}^{\prime,\mathrm{NP}})$	$(-1.61(33), 0.72(34))$	17
	$(-1.30(15), 0.53(24))$	*54*
$(C_{9,\mu}^{\mathrm{NP}}, C_{10,\mu}^{\prime,\mathrm{NP}})$	$(-1.55(32), -0.44(14))$	24
	$(-1.38(16), -0.37(12))$	*61*
$(C_{10,\mu}^{\mathrm{NP}}, C_{9,\mu}^{\prime,\mathrm{NP}})$	$(0.73(17), -0.04(24))$	17
$(C_{10,\mu}^{\mathrm{NP}}, C_{10,\mu}^{\prime,\mathrm{NP}})$	$(0.75(16), 0.04(17))$	16
$(C_{9,e}^{\mathrm{NP}}, C_{9,e}^{\prime,\mathrm{NP}})$	$(1.51(38), -0.81(37))$	10
$(C_{9,e}^{\mathrm{NP}}, C_{10,e}^{\prime,\mathrm{NP}})$	$(1.36(32), 0.87(40))$	11
$(C_{10,e}^{\mathrm{NP}}, C_{9,e}^{\prime,\mathrm{NP}})$	$(-1.06(54), -0.46(46))$	12
$(C_{10,e}^{\mathrm{NP}}, C_{10,e}^{\prime,\mathrm{NP}})$	$(-1.01(28), 0.29(29))$	12

Table 2 Values of the SMEFT WCs fit from data in all the considered scenarios along with relative ΔIC. The italic values highlight the PMD results when it can address the experimental data in a particular scenario. The PDD results are presented for all cases. For the definition of the two approaches, see Sect. 2.1

	Mean (rms)	ΔIC
C_{2223}^{LQ}	$0.75(14)$	23
	$0.79(12)$	*37*
$(C_{2223}^{LQ}, C_{2322}^{Qe})$	$(0.78(18), 0.06(32))$	21
	$(0.94(12), 0.67(17))$	*50*
$(C_{1123}^{LQ}, C_{2311}^{Qe})$	$(-0.51(29), 0.96(70))$	12
$(C_{2223}^{LQ}, C_{2223}^{ed})$	$(0.74(15), 0.16(33))$	21
	$(0.81(12), -0.19(29))$	*35*
$(C_{2223}^{LQ}, C_{2223}^{Ld})$	$(0.81(15), -0.20(15))$	22
	$(0.80(12), -0.11(12))$	*36*
$(C_{1123}^{LQ}, C_{1123}^{ed})$	$(-0.08(73), -2.1(14))$	12
$(C_{1123}^{LQ}, C_{1123}^{Ld})$	$(-0.93(27), 0.39(27))$	12
$(C_{2311}^{Qe}, C_{1123}^{ed})$	$(-0.2(18), -1.3(18))$	8
$(C_{2311}^{Qe}, C_{1123}^{Ld})$	$(1.77(47), -0.18(24))$	9

– All the angular observables and branching ratio information on $B \rightarrow K^* \mu^+ \mu^-$ from the experimental results obtained by LHCb [10,13], Belle [14], ATLAS [15] and CMS [16,17] collaborations. When available, we always take into account experimental correlations between the

measurements performed in the same bin. Note that we restrict here only to the large-recoil region, i.e. q^2 values below the J/ψ resonance, excluding measurements in the (theoretically challenging) broad-charmonium region.

– $B \to K^* e^+ e^-$ angular observables from LHCb in the available q^2 bin, [0.002, 1.12] GeV^2 [11].
– Angular observables and branching ratio of $B_s \to \phi \mu^+ \mu^-$ provided by LHCb [12].
– Branching ratio of $B_s \to \mu^+ \mu^-$ measured by LHCb [216], CMS [217], and most recently by ATLAS [218]. Note that we also employ the upper limit on $B_s \to e^+ e^-$ decay reported by HFLAV [219], useful for the study of NP coupled to electrons [83].
– Branching ratios for $B^{(+)} \to K^{(+)} \mu^+ \mu^-$ decays in the large-recoil region by LHCb [8].
– Branching ratios for the radiative decay $B \to K^* \gamma$, from HFLAV [219], and for $B_s \to \phi \gamma$ as measured by LHCb [220]. While we are not going to consider NP effects in dipole operators, these measurements are relevant in our PDD approach.
– LFUV ratios including the very recent updates: R_{K^*} in both q^2 bins, [0.045, 1.1] GeV^2 and [1.1, 6] GeV^2 [42, 169], and the R_K measurement [168].

Concerning the inputs from the theory side, our analysis is characterized in particular by the set of parameters defining form factors and non-factorizable hadronic contributions. For the former we rely on the computation presented in [178] for $B \to K^*$ and $B_s \to \phi$ amplitudes, as we take into account experimental information coming from both channels[9]; for the $B \to K$ channel, we adopt lattice QCD results extrapolated from the zero-recoil region to low-q^2 values as provided in Ref. [221]. For all the form-factor parameters adopted in this study we adopt multi-variate Gaussian distribution priors in order to include correlation matrices reported in the relevant literature.

Regarding the non-factorizable part of the amplitudes, we include hard-gluon contributions following what already outlined in detail in our previous work [166], while we proceed here differently for what regards our treatment of soft-gluon exchanges.

In the PMD approach, we do not expand Eq. (10) in powers of q^2, but we directly express it in terms of the phenomenological expression given by Eq. (7.14) of Ref. [23],[10] and we

flatly distribute all the involved parameters according to the ranges reported in table 2 of the same reference. In order to allow for imaginary parts as well, each of the three charm-loop amplitudes in Ref. [23] is multiplied by a complex phase, flatly varying each angle within $[0, 2\pi)$, yielding a total of 12 parameters to describe the non-perturbative hadronic contributions within this approach.

In the PDD approach, corresponding here to the parameterization in Eq. (11), we allow for flat priors on the absolute values of $h_\lambda^{(i)}$ coefficients and enforce as a theory weight in the likelihood the results obtained at $q^2 = 0, 1$ GeV^2 within the LCSR estimate of Ref. [23]. The following prior ranges are chosen in order to well determine the *p.d.f.* of each parameter:

$$|h_-^{(0)}| \in [0, 0.1], \quad |h_-^{(1)}| \in [0, 4], \quad |h_-^{(2)}| \in [0, 0.0001],$$
$$|h_+^{(0)}| \in [0, 0.0001], |h_+^{(1)}| \in [0, 0.0005], |h_+^{(2)}| \in [0, 0.0001],$$
$$|h_0^{(0)}| \in [0, 0.002], \quad |h_0^{(1)}| \in [0, 0.0004], \tag{22}$$

i.e. a larger range for the above priors would not alter our results. Most importantly, each of the coefficients related to the absolute values in Eq. (22) has a corresponding complex free phase. Therefore, our PDD approach is defined by a a total of 16 parameters. We used the same set of parameters in Eq. (22) to also describe the soft-gluon contributions in the case of $B_s \to \phi$, leaving possibly interesting $SU(3)_F$-breaking effects to a future investigation. Eventually, for $B \to K$ transitions we only include non-factorizable hadronic effects coming from hard-gluon exchanges, motivated by the results of Ref. [24].[11]

We conclude this section mentioning that the rest of the SM parameters varied in our analysis can be found in table 1 of Ref. [166], while for NP WCs, we adopt in general flat priors in the range $[-10, 10]$, assuming they are real. Note that some of the NP scenarios here considered showed multimodal *p.d.f.*s. In such cases we focused on the NP solution closer to the SM limit, identified by $C_i^{NP} = 0$. Finally, we point out that all our findings for the study of the SMEFT in Sect. 4 assume a NP scale set to 30 TeV. In order to read out SMEFT WCs at a different NP scale Λ, one needs to re-scale the results given in Sect. 4 appropriately.

4 EFT results from the new R_K measurement

In this section we present our results. We perform several fits to the experimental measurements listed in Sect. 3, differentiated by the set of NP WC(s) considered. We employ the PDD

---

[9] The latest LCSR update from Ref. [188], while providing an important independent cross-check of several results present in [178], does not include the estimate of $B_s \to \phi$ matrix elements.

[10] In [166] we were power-expanding h_λ correlators and enforcing the numerical results obtained from Ref. [23] in the whole large-recoil region as theory weights in the likelihood. Our new procedure for the PMD approach allows now to adopt the outcome of Ref. [23] genuinely as a set of flat priors.

[11] Nevertheless, we have tested explicitly for the case of the scenario involving $C_{9,\mu}^{NP}$ that introducing the equivalent of the PDD approach also for the $B \to K$ channel does not have a relevant impact on the results of our fit.

approach in all the scenarios examined, while exploring the PMD approach only when it can provide a satisfactory fit to current data, i.e. when NP effects built up from left-handed $b \rightarrow s$ currents coupled to vector-like (purely left-handed) muonic currents are involved in the WET (SMEFT) formalism. The goodness of the fit is here evaluated by means of the *IC*, defined in Eq. (21), while the details of the PMD and PDD approaches have been presented in Sect. 2.1.

The primary goal of this analysis consists in the study of the interplay between the new R_K measurement and NP. In particular, we investigate whether the update of R_K combined with the current R_{K^*} measurement can actually have an impact on the viable solutions to the anomalies in $b \rightarrow s$ transitions allowed by the previous R_K from Run I of LHC. To this end, we report in Tables 1 and 2 the results for the fitted values of the WCs in each of the models scrutinized here, employing the WET and the SMEFT formalism respectively. ΔIC values are also reported in the same table, marking the improvement with respect to the SM, see the discussion following Eq. (21) in Sect. 3. Finally, results for what we retain as key observables for our study are also reported in Tables 3 and 4, differentiating once again scenarios in the WET or in the SMEFT, respectively.

Our main results are illustrated here as follows. The posterior *p.d.f.*s obtained for NP coefficients are shown in Figs. 2, 3, 4, 5, 6, 7, 8 and 9. Figure 2 refers to scenarios where a single WC is taken into account. Figures 3 and 4 involve fits with two operators at the same time and correspond to two popular benchmarks previously studied in literature. Figures 5, 6, 7 and 8 correspond to 2D scenarios where NP effects in the form of $b \rightarrow s$ right-handed currents are present. Finally, in Fig. 9 the result for the largest set of SM gauge-invariant operators probed by current experimental data is presented.

For each considered scenario, we show both the posterior *p.d.f.*(s) of the NP WC(s) obtained employing the previous measurement of R_K [41], and the new one from Ref. [168]. This allows one to easily compare the impact of the new R_K measurement in our analysis. Moreover, in order to have a further insight on the role of LFUV observables as R_K and R_{K^*}, we also provide in the same figures the joint probability distribution of these ratios extracted from our fits. We give these results employing again either the 2014 measurement of R_K or its 2019 update. Our attempt is to investigate whether scenarios previously capable of addressing the anomalies in both the LFUV ratios remain viable after the R_K value recently presented in [168].

4.1 New Physics in $b \rightarrow s$ left-handed currents

Let us start our discussion examining the simple situation where the underlying BSM dynamics can be encoded in a single operator. We focus here on three different benchmarks,

namely we assume NP effects feed into a left-handed $b \rightarrow s$ current coupled to:

(i) a vectorial muonic current, i.e. $C_{9,\mu}^{\text{NP}}$;
(ii) a purely left-handed muonic current, i.e. C_{2223}^{LQ} ;
(iii) an axial electronic current, i.e. $C_{10,e}^{\text{NP}}$.

Leaving aside for a moment the role of LFUV ratios, one should note that within the PMD approach: (i) can provide an optimal outcome for the $B \rightarrow K^* \mu^+ \mu^-$ angular analysis; (ii) can provide a satisfactory description of the angular dataset (but worse than (i), being at the same time sensitive to observables as the forward-backward asymmetry measured for $B \rightarrow K^{(*)} \mu^+ \mu^-$ and the branching fraction of $B \rightarrow \mu^+ \mu^-$); (iii) badly fails to describe such a complex experimental dataset as long as one does not allow for large QCD power corrections as in the PDD approach [166].[12]

From Fig. 2 we can supplement this picture with the measurement of LFUV ratios. We note how the impact of the R_K measurement can be particularly relevant for the final outcome. Concerning case (i), we see that the interplay of R_K and R_{K^*} does not favour this scenario any longer within the 1σ regions highlighted by the orange bands in the plot. This is in contrast to the previous situation given by the 2014 measurement of R_K and represented in Fig. 2 by the vertical gray band. Most importantly, the tension arising in this NP scenario when accounting for current LFUV ratio measurements is also evident in the case of the PDD approach (right panel in the first row of the figure).

A different outcome arises from the inspection of the same Fig. 2 together with the help of the ΔIC in Tables 1 and 2 for the NP scenario (ii). In this case, the description of LFUV ratios R_K and R_{K^*} turned out to be optimal before the advent of the present R_K update. From the ΔIC value in Table 2 and the comparison with the one given in Table 1 for the scenario (i), we can conclude that in the PMD approach the operator O_{2223}^{LQ} is not so well supported by $b \rightarrow s \ell^+ \ell^-$ data. In particular, the new R_K value is not addressed within the 1σ experimental uncertainty. This fact adds to the global information arising from the rest of the observables in the fit: as a consequence, in the PMD framework NP effects in O_{2223}^{LQ} are now disfavoured with respect to contributions present in $Q_{9V,\mu}$. Interestingly, in the PDD approach the comparison between these two scenarios is completely reversed: in particular, an inspection of the corresponding ΔIC shows how allowing for larger QCD power corrections makes (ii) one of the scenarios favoured by data within the PDD framework. Indeed, the set of angular observables and the branching fraction of $B \rightarrow \mu^+ \mu^-$ can now perfectly coexist in this NP scenario; the only tension remaining in the fit of (ii) is then related to

---

[12] Electron LFUV couplings arising from a Z' mediator may be also probed by atomic-physics data [222].
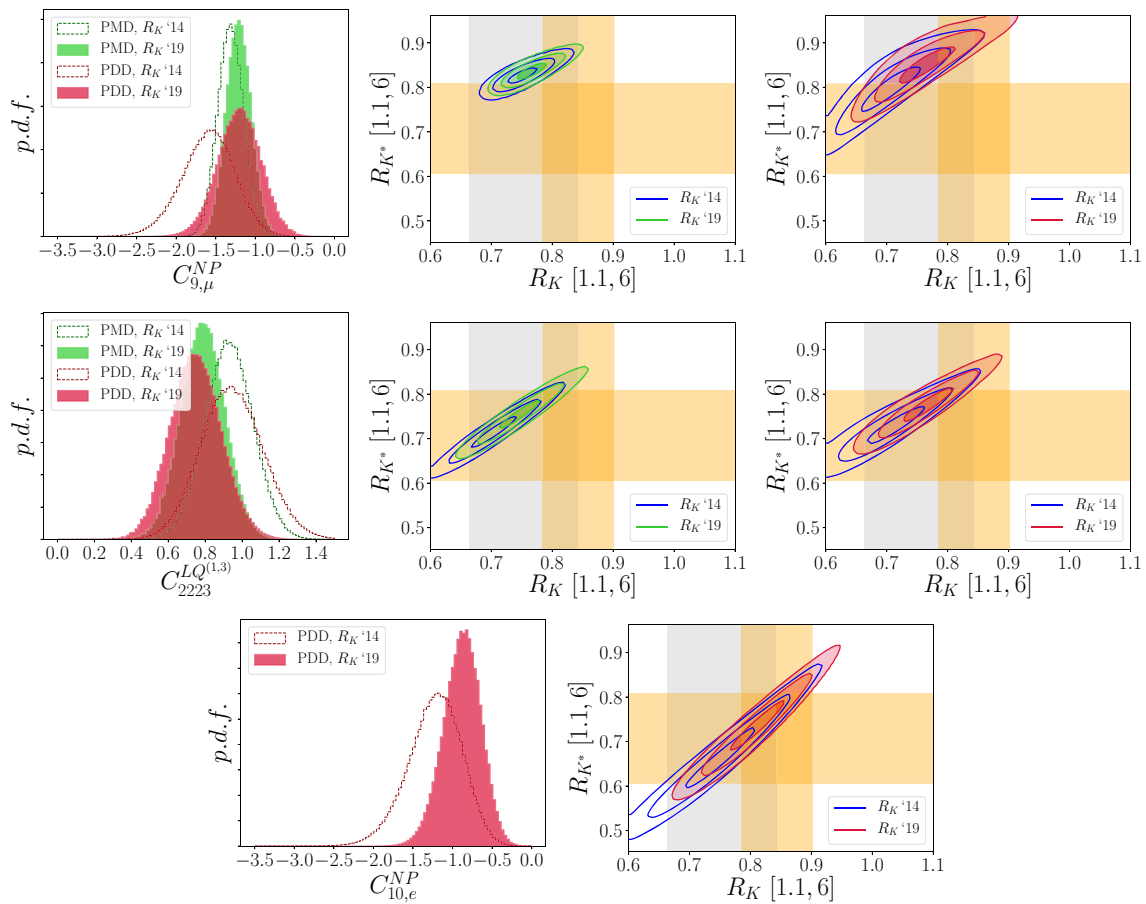
Fig. 2 First row: probability density function (p.d.f.) for the WC $C_{9,\mu}^{\mathrm{NP}}$, where the green-filled p.d.f. shows the posterior obtained in the PMD approach after the inclusion of the updated measurement for R_K, while the red-filled p.d.f. is the analogous posterior within the PDD approach (the dashed posteriors are the ones obtained employing the 2014 R_K measurement); the following panels report the combined 2D p.d.f. of the corresponding results for R_K and R_{K^*}, where the colour scheme follows the one employed in the first panel. The horizontal band corresponds to the 1σ experimental region for R_{K^*} from [42], while the two vertical bands corresponds to the previous and the current 1σ experimental regions for R_K. Second row: analogous to the first row, but relative to the WC C_{2223}^{LQ}. Third row: analogous to the first row, but relative to the WC $C_{10,e}^{\mathrm{NP}}$

this new update for R_K, shown in the right panel of central row in Fig. 2, which as of now turns out to be a very mild one.

Therefore, we wish to note that – beyond the importance of the present R_K update – the assumptions made in the size of the hadronic contributions when comparing NP scenarios turn out to be crucial. The most evident case of this sort is certainly (iii). Within a conservative approach to QCD power corrections in the $B \rightarrow K^*\ell^+\ell^-$ amplitude, this scenario offers a perfectly viable fit to $b \rightarrow s\ell^+\ell^-$ data. In particular, (iii) provides an optimal description of LFUV ratios according to what depicted in the last row of Fig. 2. However, in terms of model comparison, it remains globally disfavoured with respect to (ii) in virtue of the information arising from the angular measurements of $B \rightarrow K^*\mu^+\mu^-$. Indeed, while NP effects associated to O_{2223}^{LQ} can actually ameliorate $b \rightarrow s\ell^+\ell^-$ anomalies as the ones related to the

so-called P_5' observable [180], the phenomenological viability of NP effects encoded in the effective operator $Q_{10A,e}$ necessarily relies on large hadronic contributions [166], making (iii) a less economic alternative to (ii). This is reflected by the reported ΔIC: in the PDD approach the improvement of the SM fit provided by NP effects as in (ii) is several units of IC larger than the one provided by (iii), making (ii) much more favoured by the current experimental dataset.

As a bottom line for the inspection of NP effects in one single operator, in the PMD approach the $B \rightarrow K^*\mu^+\mu^-$ angular analysis still greatly favours the presence of NP effects from $Q_{9V,\mu}$, while more NP scenarios are viable with a more conservative approach to QCD power corrections, and a particularly favoured one turns out to be O_{2223}^{LQ}. Finally, we observe how the three scenarios discussed so far may be distinguished with a future measurement of transverse and longitudinal ratios in the q^2-bin [1.1, 6], quite

Fig. 3 2D p.d.f. for the scenario with WCs $(C_{9,\mu}^{\mathrm{NP}}, C_{9,e}^{\mathrm{NP}})$ and combined 2D p.d.f. of the corresponding results for R_K and R_{K^*} in both the PMD and the PDD approaches, following the colour scheme defined below Fig. 2. In order to highlight the role of LFUV observables in this scenario we show in the left panels the WCs in the $\mu \pm e$ combination
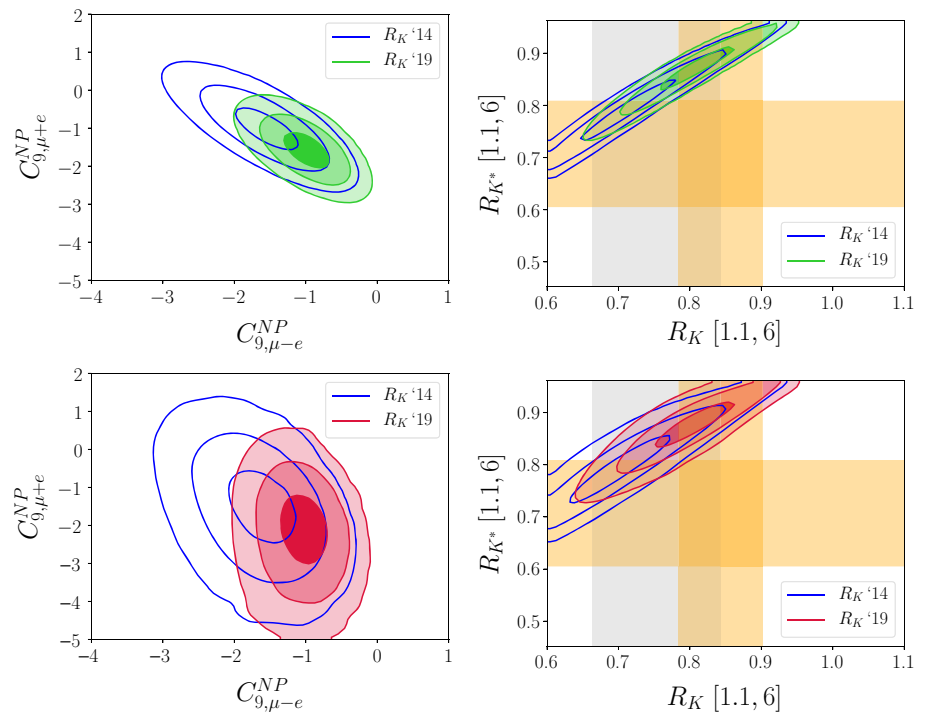
robust against hadronic uncertainties, see Tables 3 and 4. Among (i), (ii), (iii) $R_{K^*,\phi}^{\mathrm{T}}[1.1, 6] \simeq 1.0$ would favour NP effects from $Q_{9V,\mu}$, while $R_{K^*,\phi}^{\mathrm{T}}[1.1, 6] \simeq 0.8$ would point to BSM dynamics in O_{2223}^{LQ}, and a measurement of $R_{K^*,\phi}^{\mathrm{T}}[1.1, 6] \simeq 0.7$ would hint at NP in $Q_{10A,e}$.

Let us now turn to the investigation of more complex cases, where BSM dynamics is actually described by a pair of effective operators rather than just a single one. We start focussing on the scenario where the effective couplings of interest turn out to be $(C_{9,\mu}^{\mathrm{NP}}, C_{9,e}^{\mathrm{NP}})$. Note from Table 1 that the addition of a NP contribution coming from the electron operator $Q_{9V,e}$ does not strongly improve the fit obtained with $Q_{9V,\mu}$: in terms of ΔIC, both PMD and PDD approaches slightly penalize this scenario, underlying a marginal improvement in the description of current data in correspondence to the addition of $C_{9,e}^{\mathrm{NP}}$. This is also captured by the LFUV ratios in the right panels of Fig. 3, where an improvement is only seen in the value of R_K. Moreover, the prediction for longitudinal and transverse components of $R_{K^*,\phi}$ remain essentially the same for the two scenarios 3.

Nevertheless, this NP benchmark is particularly illustrative of a study case where a robust estimate of NP effects – i.e. as much orthogonal to hadronic effects as possible – is actually feasible. It is indeed instructive to recast this case in the basis where NP effective couplings come into the linear combinations $(C_{9,\mu-e}^{\mathrm{NP}}, C_{9,\mu+e}^{\mathrm{NP}})$. As already discussed in Sects. 2.1–2.3 and highlighted e.g. in Refs. [39,223], such a choice is naturally driven by the presence of LFUV observables in the fit, that are maximally sensitive to $\mu - e$ combination at the linear level in the NP WCs for Q_{9V}. At the

same time, the $\mu - e$ combination is by definition free from hadronic uncertainties of any sort and the determination of this effective coupling signals unambiguously the presence of NP, regardless of the approach chosen for the inclusion of hadronic contributions in the analysis. The independence from the approach taken for QCD power corrections is evident from the comparison of the two panels on the left column of Fig. 3: going from the PMD to the PDD approach, NP in the $\mu + e$ direction gets diluted by hadronic effects, while the determination of the $\mu - e$ WC consistently differs from 0 at more than 3σ.

We then move to the inspection of cases where heavy new degrees of freedom can generically couple the left-handed $b \to s$ current to both vectorial and axial leptonic structures or, from the BSM perspective drawn in the SMEFT, to both left-handed and right-handed leptonic currents. These NP scenarios generalize the specific benchmarks (i), (ii), (iii) discussed at the beginning of the section. Left and central columns in Fig. 4 report the result for the PMD and PDD approach in the case where NP effects lie in the muonic mode only, while the PDD approach for the case of the electronic mode is given in the right column. Comparing with what already illustrated for (i), (ii), (iii), with the help of Table 2 and the second row of Fig. 4 we can easily conclude that NP contributions from $O_{2223}^{LQ} - O_{2322}^{Qe}$ are still favoured by data, slightly improving the description of R_K with respect to the minimal case (i) in the PMD approach, and the minimal case (ii) in the PDD approach. Moreover, the case where NP effects arise from the pair $O_{1123}^{LQ} - O_{2311}^{Qe}$ is not favoured over the simpler axial electronic proposal
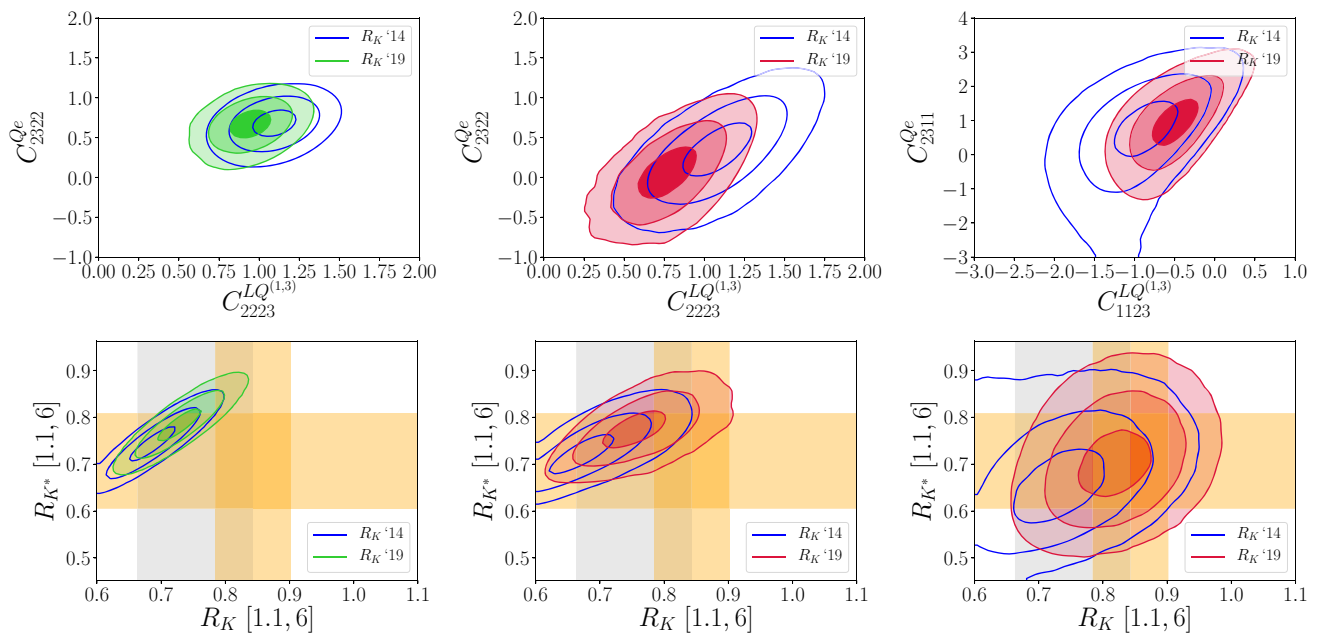
Fig. 4 2D p.d.f. for the scenario with WCs (C_9^{NP}, C_{10}^{NP}) and combined 2D p.d.f. of the corresponding results for R_K and R_{K^*} in both the PMD and the PDD approaches, following the colour scheme defined below

Fig. 2. We show the result in the SM gauge-invariant language, for both the muonic (left and central column) and electronic (right column) case
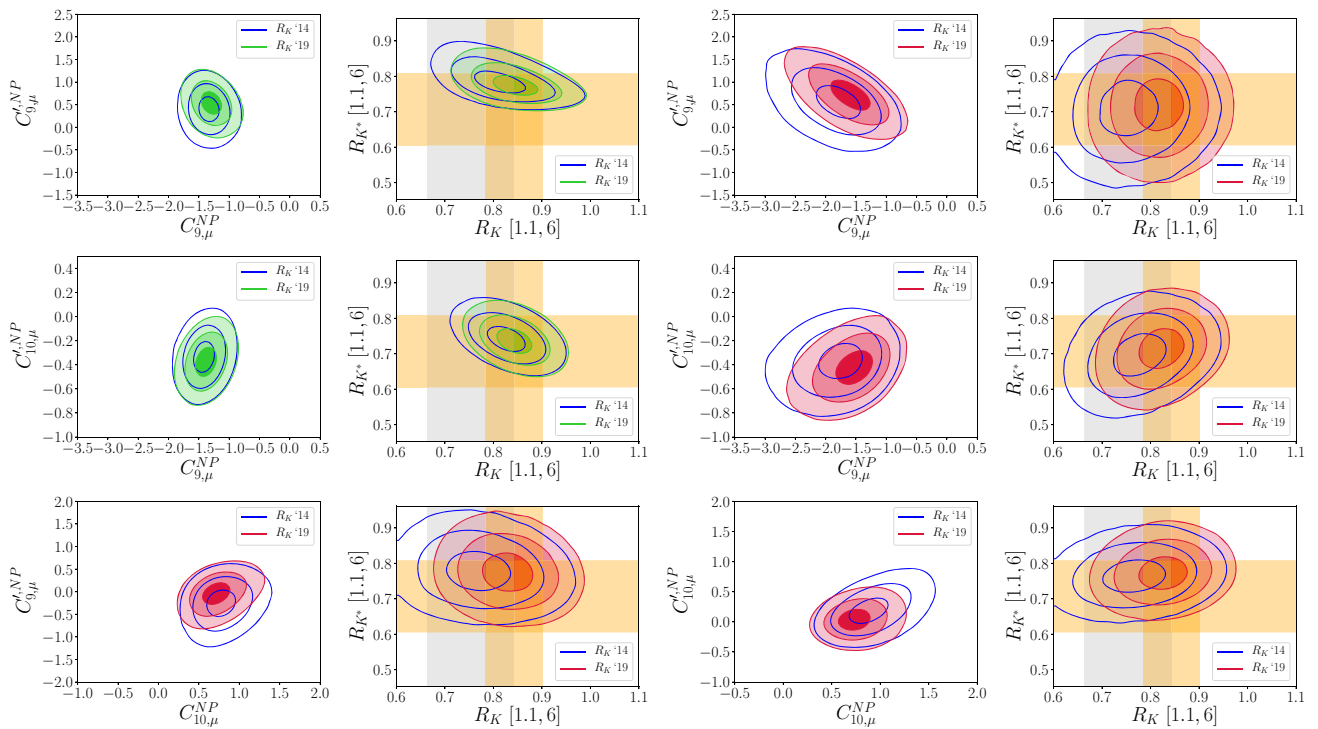

Fig. 5 First row: 2D p.d.f. for the scenario with WCs $(C_{9,\mu}^{NP}, C_{9,\mu}^{',NP})$ and combined 2D p.d.f. of the corresponding results for R_K and R_{K^*} in both the PMD and the PDD approaches, following the colour scheme defined below Fig. 2. Second row: analogous to the first row, but rel-

ative to the WCs $(C_{9,\mu}^{NP}, C_{10,\mu}^{',NP})$. Third row: analogous to the first row, but in the PDD approach only and relative to the WCs $(C_{10,\mu}^{NP}, C_{9,\mu}^{',NP})$ and $(C_{10,\mu}^{NP}, C_{10,\mu}^{',NP})$

denoted here as (iii). Interestingly, from Table 4 we can also observe that a measurement of the transverse component of the ratios $R_{K*,\phi}$ for these scenarios would be quite indicative. Indeed, the prediction of these LFUV observables from NP effects in O_{2223}^{LQ}–O_{2322}^{Qe} points to $R_{K*,\phi}^{\mathrm{T}}[1.1,6] \simeq 0.95$ and $R_{K*,\phi}^{\mathrm{T}}[1.1,6] \simeq 0.85$ in the PMD and PDD approach respectively, compatible among each other only at the 1σ level, and different from the ones obtained for (i) and (ii). On the contrary, the corresponding LFUV prediction from the electronic pair considered here would not be distinguishable from what assessed already in (iii). Finally, from the same Table 4 we also highlight that the study of NP effects from the full set of four operators $O_{\ell\ell23}^{LQ}$–$O_{23\ell\ell}^{Qe}$ with $\ell = \{1, 2\}$, would not change the important phenomenological interplay found for the pair O_{2223}^{LQ}–O_{2322}^{Qe}, but would quite distinctively predict transverse ratios $R_{K*,\phi}^{\mathrm{T}}[1.1,6] \simeq 0.75$, independently of the hadronic approach considered. We postpone a thorough discussion on the analysis of these four operators all together to Appendix B, where we study them in the context of the loop-generated effects reported in Eq. (15), and where we also emphasize the possible connections of $b \to s\ell^+\ell^-$ anomalies with EW precision physics [199,200,207].

4.2 New Physics in both $b \to s$ left- and right-handed currents

We continue our discussion of 2D scenarios reaching one of the highlights of this study in relation to the new R_K measurement and what outlined in Sect. 2.3: the investigation of NP effects entering both $b \to s$ left-handed and right-handed currents in dimension-six semileptonic operators. Indeed, from the discussion following Eq. (20) we recall that as long as R_{K*} can be retained to have a role quite complementary to the one of R_K as a probe of NP, the new measurement appearing in Eq. (1) – supplemented by the current one for R_{K*} in the same bin of q^2 – hints at new heavy degrees of freedom coupled to $b \to s$ right-handed currents. As we show in what follows, this conclusion remains subject to the taming of non-factorizable hadronic contributions.

We start by considering NP effects in vectorial and axial muonic currents and described by means of the WET formalism, namely the pairs of NP WCs: $(C_{9,\mu}^{\mathrm{NP}}, C_{9,\mu}^{\prime,\mathrm{NP}})$, $(C_{9,\mu}^{\mathrm{NP}}, C_{10,\mu}^{\prime,\mathrm{NP}})$, $(C_{10,\mu}^{\mathrm{NP}}, C_{9,\mu}^{\prime,\mathrm{NP}})$ and $(C_{10,\mu}^{\mathrm{NP}}, C_{10,\mu}^{\prime,\mathrm{NP}})$. The two former scenarios are generalizations of the study case (i), and are allowed both in the PMD and PDD approaches, while the latter two can satisfactorily address $b \to s\ell^+\ell^-$ anomalies only within the PDD approach. Results for all these scenarios can be found in Fig. 5. As first highlighted by the trend in the reported ΔIC and further depicted by R_K–R_{K*} plots, the inclusion of right-handed $b \to s$ effective couplings allows for an overall better description of data. In particular, from the inspection of the central row in Fig. 5 the scenario involving

the operators $Q_{9V,\mu}$ and $Q_{10A,\mu}'$ provides the best match here to the newly measured R_K together with R_{K*} in the q^2-bin $[1.1,6]$ GeV^2. Moreover, it yields an optimal description of $B_s \to \mu^+\mu^-$ and of the whole angular analysis at the same time – independently of the hadronic approach undertaken – and hence stands out in Table 1 as the study case with the highest ΔIC in both PMD and PDD approaches. This result comes together with the prediction for $R_{K*,\phi}^{\mathrm{T}}[1.1,6] \simeq 1$ in the scenarios with the pairs $Q_{9V,\mu}$–$Q_{9V(10A),\mu}'$. We also note that the prediction of the longitudinal ratio unfortunately does not allow to single out within errors the NP case of $Q_{9V,\mu}$–$Q_{9V,\mu}'$ with respect to $Q_{9V,\mu}$–$Q_{10,\mu}'$.

A different prediction for the transverse and longitudinal LFUV ratios is instead obtained for the pairs $Q_{10A,\mu}$–$Q_{9V(10A),\mu}'$, approximately giving $R_{K*,\phi}^{\mathrm{T}}[1.1,6] \simeq R_{K*,\phi}^{\mathrm{L}}[1.1,6] \simeq 0.75$. We note that the non-trivial interplay between hadronic physics – addressing here the $B \to K^*\mu^+\mu^-$ angular analysis – and the experimental weights of the measured LFUV ratios and of $Br(B_s \to \mu^+\mu^-)$ lead overall to a lower ΔIC value for these two scenarios with respect to the case of $Q_{9V,\mu}$ and $Q_{10A,\mu}'$ (see Table 1).

A similar very good description of measured LFUV ratios is also obtained in the 2D scenarios with NP effects in the electron channel only, described by means of the WET formalism, namely $(C_{9,e}^{\mathrm{NP}}, C_{9,e}^{\prime,\mathrm{NP}})$, $(C_{9,e}^{\mathrm{NP}}, C_{10,e}^{\prime,\mathrm{NP}})$, $(C_{10,e}^{\mathrm{NP}}, C_{9,e}^{\prime,\mathrm{NP}})$ and $(C_{10,e}^{\mathrm{NP}}, C_{10,e}^{\prime,\mathrm{NP}})$. In these scenarios, NP cannot provide a satisfactory explanation of the angular dataset for the $B \to K^*\mu^+\mu^-$ decay: therefore, they are viable only within the PDD approach. Results for these scenarios are reported in Fig. 6, that capture indeed the very good description of R_{K*}–R_K in the q^2-bin $[1.1,6]$ GeV^2 in all the four cases at hand. However, comparing the ΔIC in Table 1, none of these models turns out to be competitive with NP effects coming from $Q_{9V,\mu}$–$Q_{10A,\mu}'$ operators. Looking again at Table 3, one can still find a particular footprint of these scenarios via the prediction of longitudinal and transverse ratios. In particular, the two cases where $C_{9,e}^{\mathrm{NP}}$ is involved predict a quite large transverse ratio, $R_{K*,\phi}^{\mathrm{T}}[1.1,6] \simeq 0.95$, while the two scenarios where $C_{10,e}^{\mathrm{NP}}$ is present point to $R_{K*,\phi}^{\mathrm{T}}[1.1,6] \simeq 0.7$. The four scenarios here discussed qualitatively go along with the same picture drawn for the pairs $Q_{10A,\mu}$–$Q_{9V(10A),\mu}'$: they turn out to be less competitive than the case of $Q_{9V,\mu}$ and $Q_{10A,\mu}'$.

We now proceed considering NP effects in left-handed and right-handed muonic currents employing the gauge-invariant language of the SMEFT. In particular, we first focus on the scenarios $(C_{2223}^{LQ}, C_{2223}^{ed})$ and $(C_{2223}^{LQ}, C_{2223}^{Ld})$, that are generalizations of the study case *ii)*, therefore viable both in the PMD and in the PDD approach. Their results are shown in Fig. 7. Similarly to what found above for the pairs $Q_{10A,\mu}$–$Q_{9V(10A),\mu}'$ and $Q_{9V(10A),e}$–$Q_{9V(10A),e}'$, in these scenarios – in spite of the R_K update – the presence of right-handed
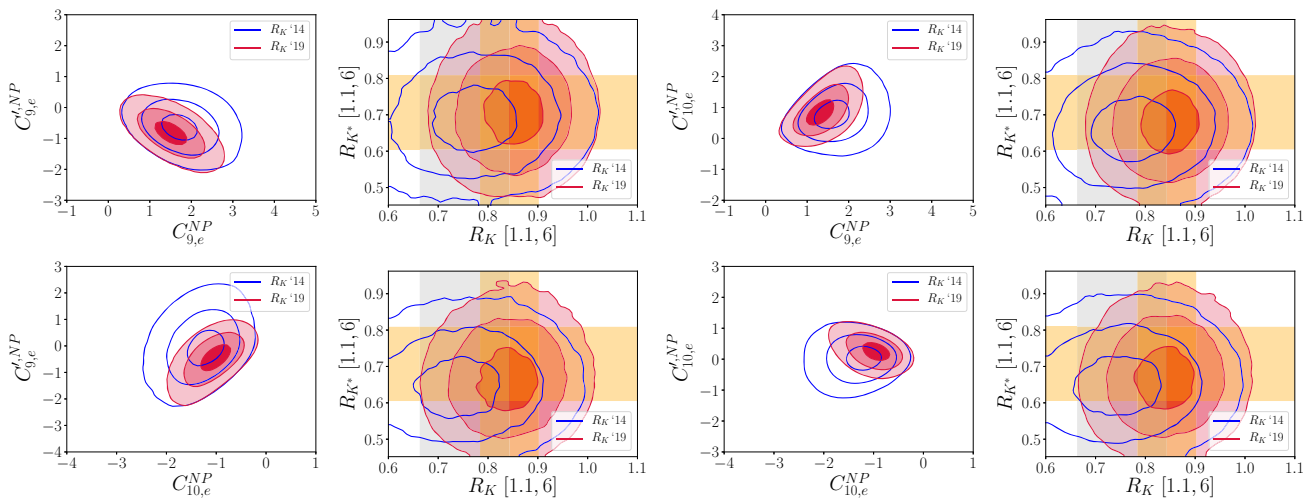
Fig. 6 First row: the first two panels show 2D p.d.f. for the scenario with WCs $(C_{9,e}^{\mathrm{NP}}, C_{9,e}^{\prime,\mathrm{NP}})$ and the combined 2D p.d.f. of the corresponding results for R_K and R_{K^*} in the PDD approaches, following the colour scheme defined below Fig. 2, while the last two panels show the same for the scenario with WCs $(C_{9,e}^{\mathrm{NP}}, C_{10,e}^{\mathrm{NP}})$. Second row: analogous to the first row, but relative to the WCs $(C_{10,e}^{\mathrm{NP}}, C_{9,e}^{\prime,\mathrm{NP}})$ and $(C_{10,e}^{\mathrm{NP}}, C_{10,e}^{\prime,\mathrm{NP}})$
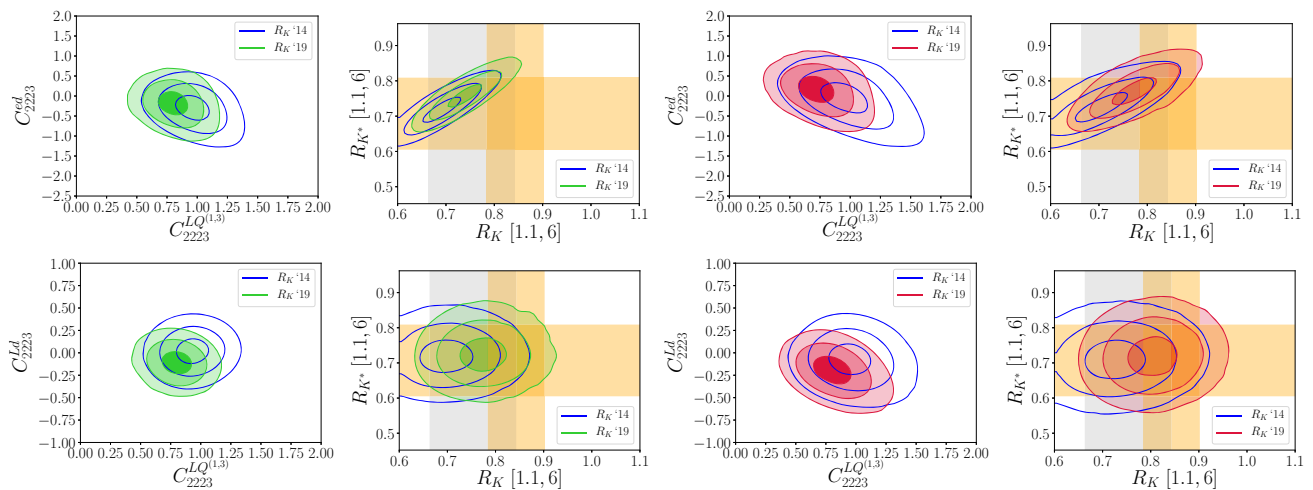
Fig. 7 First row: 2D p.d.f. for the scenario with WCs $(C_{2223}^{LQ}, C_{2223}^{ed})$ and combined 2D p.d.f. of the corresponding results for R_K and R_{K^*} in both the PMD and the PDD approaches, following the colour scheme defined below Fig. 2. Second row: analogous to the first row, but relative to the WCs $(C_{2223}^{LQ}, C_{2223}^{Ld})$

currents has an overall marginal phenomenological impact. These conclusions are corroborated by the values of ΔIC, slightly penalizing these scenarios in comparison with the study case (ii): a marginal improvement in the description of data is indeed obtained at the cost of model complexity in the fit. We eventually point out that the prediction for the longitudinal and transverse LFUV ratios are quite similar within these NP cases, yielding in particular $R_{K^*,\phi}^{\mathrm{T}}[1.1, 6] \simeq 0.8$.

In the spirit of studying the interplay between left-handed and right-handed currents in the SMEFT framework, one may investigate also the viability of the above scenarios replacing the role carried out by O_{2223}^{LQ} with the one of O_{2322}^{Qe}. However, Eq. (19) implies that the 2D scenario $(C_{2322}^{Qe}, C_{2223}^{ed})$ cannot explain the measured value of R_K, since both coefficients

contribute to the ratio with upward shifts, in contrast with what is required to account for the experimental data. On the other hand, considering C_{2223}^{Ld} as the NP term responsible of effects stemming from right-handed currents, positive solutions for this coefficient produce downward shifts in R_K, potentially making the $(C_{2322}^{Qe}, C_{2223}^{Ld})$ scenario a viable solution for this LFUV ratio, see right panel in Fig. 1. However, as shown e.g. in Ref. [162], downward shifts in R_K induced by C_{2223}^{Ld} correspond to upward shifts in R_{K^*}: therefore, since C_{2322}^{Qe} always contributes positively to this second ratio as well, also this second scenario cannot be considered viable in order to simultaneously address the anomalies in the two LFUV ratios.
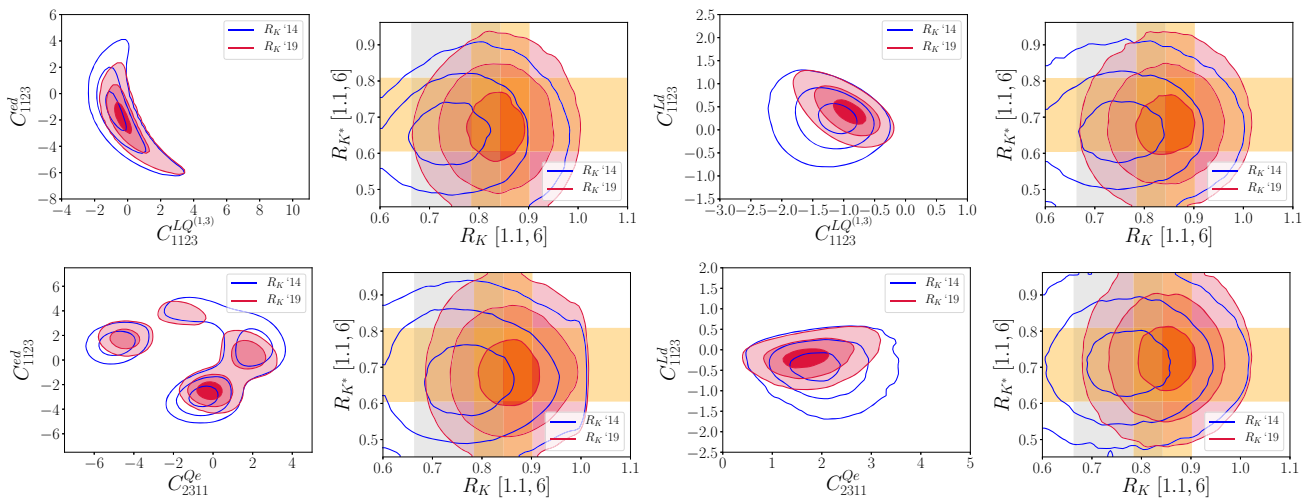
Fig. 8 First row: the first two panels show 2D p.d.f. for the scenario with WCs $(C_{1123}^{LQ^{(1,3)}}, C_{1123}^{ed})$ and the combined 2D p.d.f. of the corresponding results for R_K and R_{K^*} in the PDD approaches, following the colour scheme defined below Fig. 2, while the last two panels show the same for the scenario with WCs $(C_{1123}^{LQ^{(1,3)}}, C_{1123}^{Ld})$. Second row: analogous to the first row, but relative to the WCs $(C_{2311}^{Qe}, C_{1123}^{ed})$ and $(C_{2311}^{Qe}, C_{1123}^{Ld})$.

Similar results are obtained in the last set of 2D scenarios, involving NP effects in electron channel described by means of the SMEFT formalism, namely $(C_{1123}^{LQ}, C_{1123}^{ed})$, $(C_{1123}^{LQ}, C_{1123}^{Ld})$, $(C_{2311}^{Qe}, C_{1123}^{ed})$ and $(C_{2311}^{Qe}, C_{1123}^{Ld})$. It is interesting to note that, contrarily to what observed for the corresponding muonic case, both scenarios involving the operator O_{2311}^{Qe} are here allowed, due to the opposite direction of the contribution induced by such operator in the electron sector as shown in Eq. (19). Once again, addressing the information stemming from the angular dataset for the $B \to K^* \mu^+ \mu^-$ decay requires these scenarios to be considered only in the PDD approach. The results for these fits, reported in Fig. 8, show a good description of R_K and R_{K^*} in all the considered cases. However, once again the ΔIC values reported in Table 2 imply that none of these models is favoured in comparison with the scenarios featuring NP effects in O_{2223}^{LQ}.

We conclude this section briefly discussing the case where all the SMEFT operators are inspected all together. Indeed, the experimental dataset at hand allows us to perform a fit for NP effects present in all the 12 tree-level SMEFT operators, switching on simultaneously the following effective couplings: $C_{\ell\ell23}^{LQ}$, $C_{23\ell\ell}^{Qe}$, $C_{\ell\ell23}^{Ld}$, $C_{\ell\ell23}^{ed}$, $C_{\ell\ell23}^{LedQ}$ and $C_{\ell\ell23}^{'LedQ}$, with $\ell = \{1, 2\}$. For the sake of completeness, in this scenario we also include scalar operators, particularly constrained by the available experimental information on $B_s \to \ell^+\ell^-$. We report the results of our fit in the PMD and PDD approaches in Fig. 9. Most importantly, we observe that in both approaches C_{2223}^{LQ} is found to be different from 0: at the $\sim 6\sigma$ level in the PMD approach, at more than 3σ in the PDD one. For the PMD framework we also note that NP effects in O_{2322}^{Qe} are singled out at the $\sim 5\sigma$ level. These findings pretty much

reflect what already outlined from Table 2, where the preferred scenario in the PDD approach is indeed the one featuring only C_{2223}^{LQ}, while in the case of a more aggressive approach to QCD power corrections one needs to require also the presence of C_{2322}^{Qe} in order to accomplish an overall good description of data within the SMEFT. It is finally worth pointing out that the results of key observables as longitudinal and transverse LFUV ratio reported in Table 4 are here compatible with $R_{K^*,\phi}^{\mathrm{T,L}}[1.1, 6] \simeq 0.7$ within 1σ errors.

5 Conclusions

In this study we investigated the impact of the very recent R_K and R_{K^*} measurements on New Physics (NP) in $b \to s\ell^+\ell^-$ transitions. We focused on the study of NP effects related to Lepton Flavour Universality violation (LFUV). We have explicitly shown that an aggressive or conservative approach to hadronic matrix elements may drastically modify the conclusions drawn from the updated $b \to s\ell^+\ell^-$ global analysis. A set of key messages can be extracted from our comprehensive study:

– in the considered "WET scenarios", i.e. the cases where NP contributions do not necessarily stem a priori from $SU(2)_L \otimes U(1)_Y$ gauge-invariant operators at high energies, a preference for NP coupled to both left-handed quark currents with vector muon coupling and to right-handed quark currents with axial muon coupling stands out regardless of the treatment of hadronic uncertainties;

– in the instance of "SMEFT scenarios", namely when NP effects are explicitly correlated by $SU(2)_L \otimes U(1)_Y$ gauge invariance in the UV, several distinct cases are able to address present experimental information depending on the treatment of hadronic effects undertaken; aggressive estimates of hadronic uncertainties point to the simultaneous presence of left-handed quark and muon couplings and left-handed quark and right-handed muon couplings; a more conservative analysis leaves room for a broader set of scenarios, including the case of the single purely left-handed operator with muon coupling;

– LFUV effects in the electron sector provide a good description of current $R_{K^{(*)}}$ measurements, but an overall satisfactory description of experimental results can be obtained only within a conservative approach to QCD effects; within this framework, these NP scenarios are not favoured over ones featuring muon couplings.

We look forward to strengthening and improving our conclusions with the help of forthcoming experimental results: (a) novel LFUV data from $B_s \to \phi\ell^+\ell^-$, that would corroborate the current ones for $B \to K^*\ell^+\ell^-$; (b) possible measurements of LFUV ratios as $R_{K^*,\phi}^{\mathrm{T,L}}$ in the q^2-bin [1.1,6] GeV^2, that may help to further disentangle the different NP effects highlighted in this work, see Tables 3 and 4; (c) new measurements of lepton-flavour dependent angular observables as in Ref. [14], that would also help to single out heavy new dynamics from standard hadronic physics.

Appendix A: highlights on current and future measurements

In this appendix we collect a subset of the interesting measurements related to the set of $b \to s\ell^+\ell^-$ anomalies, namely R_K, R_{K^*} (for this one both low-q^2 bin, [0.045,1.1] GeV^2, and the central one, [1.1,6] GeV^2), and the two interesting bins of P_5' falling in the region towards the J/ψ resonance. Most importantly, we show the prediction in the q^2 bin [1.1,6] relative to R_ϕ and to the transverse and longitudinal ratios $R_{K^*}^{\mathrm{T,L}}$ and $R_\phi^{\mathrm{T,L}}$. In the first row of Tables 3 and 4 we report the experimental measurement (when available), with statistical and systematic errors combined and symmetrized. In particular, concerning both bins of R_{K^*} and the critical bins of P_5', we limit ourselves to report the experimental measurements of LHCb only, the most precise ones currently available for these observables. In the following rows, we give the values obtained for each of the mentioned observables in all the scenario described in Sect. 4. Table 3 is relative to the scenarios investigated within the WET framework, while Table 4 refers to the ones described within the SMEFT framework.

Appendix B: Top-quark operators for $b \to s\ell^+\ell^-$ anomalies

As anticipated in Sect. 2.2, in this appendix we detail the fit results for the interesting scenario related to loop-generated effects relevant for $b \to s\ell^+\ell^-$ anomalies from dimension-six gauge-invariant effective operators involving right-handed top quarks, see Eq. (17).

The SMEFT operators of interest enter in our analysis according to the matching condition reported in Eq. (15): they do not mix into WET operators with right-handed $b \to s$ currents, but contribute only to WCs of $Q_{9V,10A}$. Consequently, a quite important observation can be drawn from what is already illustrated in Sect. 2.3: the new R_K measurement, on general grounds, disfavours scenarios with WET operators involving only left-handed $b \to s$ currents. As we found in Sect. 4, it is nevertheless important to note that once hadronic corrections are treated conservatively, such a hint for NP contributions to primed operators in the WET gets weakened. Hence, $C_{9,10}^{\mathrm{NP}}$ effects from top-quark loops remain particularly appealing in light of the new R_K measurement.

The fit of the full set of top-quark SMEFT operators involved is shown in Fig. 10. In green we show the result within the PMD approach, while in red we present the PDD one. In the former approach, we find evidence for NP at more than the 6σ level in the operator O_{2233}^{Lu}, together with the far-reaching evidence for a non-zero contribution from O_{2233}^{eu}

Fig. 9 Global fit of all tree-level SMEFT WCs ($\Lambda = 30\ TeV$) constrained by $b \to s\ell^+\ell^-$ measurements within the PMD (green) and PDD (red) approach, including the 2019 R_K measurement. 16-th, 50-th, 84-th percentile for marginalized distributions is reported

Table 3 Experimental measurements with symmetrized errors (for R_{K^*} and P_5' we report the LHCb ones) and results from the fit for key observables in the WET scenarios considered here. The italic values highlight the PMD results when experimental data can be well described within the approach. The PDD results are presented for all cases. For the definition of the two approaches, see Sect. 2.1

Exp.	$R_K[1.1, 6]$ 0.850(59)	$R_{K^*}[0.045, 1.1]$ 0.680(93)	$R_{K^*}[1.1, 6]$ 0.71(10)	$P_5'[4, 6]$ $-0.30(16)$	$P_5'[6, 8]$ $-0.51(12)$	$R_{K^*}^T[1.1, 6]$ –	$R_{K^*}^L[1.1, 6]$ –	$R_\phi[1.1, 6]$ –	$R_\phi^T[1.1, 6]$ –	$R_\phi^L[1.1, 6]$ –
$C_{9,\mu}^{NP}$	0.762(43)	0.889(12)	0.845(38)	$-0.441(59)$	$-0.558(76)$	1.032(22)	0.783(48)	0.851(39)	1.039(25)	0.787(48)
	0.767(25)	*0.889(8)*	*0.833(17)*	*$-0.472(46)$*	*$-0.616(43)$*	*1.029(15)*	*0.771(25)*	*0.838(18)*	*1.037(20)*	*0.773(25)*
$C_{10,e}^{NP}$	0.807(46)	0.841(23)	0.733(58)	$-0.462(59)$	$-0.552(77)$	0.726(58)	0.736(59)	0.732(59)	0.729(57)	0.733(60)
$(C_{9,\mu}^{NP}, C_{9,e}^{NP})$	0.802(56)	0.895(13)	0.869(45)	$-0.436(59)$	$-0.564(76)$	1.036(22)	0.812(57)	0.874(45)	1.042(25)	0.816(57)
	0.807(56)	*0.896(12)*	*0.865(44)*	*$-0.456(50)$*	*$-0.606(44)$*	*1.030(16)*	*0.810(55)*	*0.869(44)*	*1.037(20)*	*0.813(55)*
$(C_{9,\mu}^{NP}, C_{9,\mu}'^{NP})$	0.818(51)	0.828(34)	0.708(72)	$-0.445(60)$	$-0.561(79)$	1.042(47)	0.619(80)	0.714(74)	1.045(50)	0.623(81)
	0.845(46)	*0.860(16)*	*0.771(28)*	*$-0.471(47)$*	*$-0.627(44)$*	*1.050(24)*	*0.690(38)*	*0.779(28)*	*1.054(26)*	*0.695(37)*
$(C_{9,\mu}^{NP}, C_{10,\mu}'^{NP})$	0.822(46)	0.831(25)	0.703(57)	$-0.459(61)$	$-0.567(79)$	1.016(29)	0.617(63)	0.712(57)	1.029(34)	0.620(64)
	0.845(35)	*0.845(17)*	*0.731(36)*	*$-0.497(48)$*	*$-0.646(45)$*	*1.024(18)*	*0.649(43)*	*0.739(35)*	*1.039(23)*	*0.650(44)*
$(C_{10,\mu}^{NP}, C_{9,\mu}'^{NP})$	0.831(52)	0.859(22)	0.774(55)	$-0.482(64)$	$-0.552(83)$	0.755(43)	0.782(64)	0.776(54)	0.764(42)	0.781(63)
$(C_{10,\mu}^{NP}, C_{10,\mu}'^{NP})$	0.826(50)	0.859(18)	0.773(46)	$-0.483(64)$	$-0.553(83)$	0.752(42)	0.781(53)	0.775(46)	0.761(40)	0.780(53)
$(C_{9,e}^{NP}, C_{9,e}'^{NP})$	0.853(59)	0.818(41)	0.697(88)	$-0.453(60)$	$-0.540(78)$	0.972(56)	0.622(95)	0.705(89)	0.984(59)	0.628(96)
$(C_{9,e}^{NP}, C_{10,e}'^{NP})$	0.851(58)	0.809(41)	0.671(86)	$-0.456(60)$	$-0.544(78)$	0.923(59)	0.601(90)	0.676(87)	0.942(59)	0.602(91)
$(C_{10,e}^{NP}, C_{9,e}'^{NP})$	0.840(60)	0.813(43)	0.670(85)	$-0.464(59)$	$-0.555(77)$	0.682(68)	0.652(94)	0.670(84)	0.685(68)	0.650(93)
$(C_{10,e}^{NP}, C_{10,e}'^{NP})$	0.841(60)	0.806(42)	0.663(85)	$-0.465(59)$	$-0.557(77)$	0.688(66)	0.654(95)	0.663(85)	0.693(66)	0.651(96)

Table 4 Experimental measurements with symmetrized errors (for R_{K^*} and P_5' we report the LHCb ones) and results from the fit for key observables in the SMEFT scenarios considered here. The italic values highlight the PMD results when experimental data can be well described within the approach. The PDD results are presented for all cases. For the definition of the two approaches, see Sect. 2.1

| Exp.	$R_K[1.1, 6]$ 0.850(59)	$R_{K^*}[0.045, 1.1]$ 0.680(93)	$R_{K^*}[1.1, 6]$ 0.71(10)	$P_5'[4, 6]$ $-0.30(16)$	$P_5'[6, 8]$ $-0.51(12)$	$R_{K^*}^T[1.1, 6]$ –	$R_{K^*}^L[1.1, 6]$ –	$R_\phi[1.1, 6]$ –	$R_\phi^T[1.1, 6]$ –	$R_\phi^L[1.1, 6]$ –
C_{2223}^{LQ}	0.764(41)	0.860(13)	0.771(38)	$-0.471(63)$	$-0.555(83)$	0.836(30)	0.748(40)	0.775(37)	0.846(29)	0.749(41)
	0.746(36)	*0.857(12)*	*0.754(34)*	*$-0.670(28)$*	*$-0.764(30)$*	*0.799(28)*	*0.741(36)*	*0.754(34)*	*0.803(27)*	*0.739(36)*
$(C_{2223}^{LQ}, C_{2322}^{Qe})$	0.760(49)	0.860(14)	0.770(39)	$-0.469(63)$	$-0.556(82)$	0.844(64)	0.744(42)	0.774(39)	0.855(64)	0.745(42)
	0.728(34)	*0.871(13)*	*0.781(36)*	*$-0.511(53)$*	*$-0.650(47)$*	*0.947(51)*	*0.729(35)*	*0.784(36)*	*0.957(52)*	*0.731(35)*
$(C_{1123}^{LQ}, C_{2311}^{Qe})$	0.819(55)	0.827(32)	0.705(72)	$-0.469(60)$	$-0.560(77)$	0.68(11)	0.720(63)	0.703(74)	0.68(11)	0.715(65)
$(C_{2223}^{LQ}, C_{2223}^{ed})$	0.773(46)	0.858(14)	0.767(38)	$-0.472(63)$	$-0.552(82)$	0.839(31)	0.742(42)	0.771(38)	0.851(30)	0.742(42)
	0.738(37)	*0.858(12)*	*0.758(34)*	*$-0.653(38)$*	*$-0.754(34)$*	*0.804(28)*	*0.744(36)*	*0.758(34)*	*0.806(27)*	*0.743(36)*
$(C_{2223}^{LQ}, C_{2223}^{Ld})$	0.805(52)	0.834(24)	0.714(56)	$-0.478(64)$	$-0.547(83)$	0.819(35)	0.680(63)	0.719(55)	0.831(34)	0.681(63)
	0.775(49)	*0.842(20)*	*0.724(47)*	*$-0.693(38)$*	*$-0.786(39)$*	*0.792(29)*	*0.704(53)*	*0.724(47)*	*0.796(28)*	*0.702(53)*
$(C_{1123}^{LQ}, C_{1123}^{ed})$	0.837(59)	0.819(44)	0.672(90)	$-0.463(59)$	$-0.553(77)$	0.71(10)	0.644(90)	0.670(92)	0.726(99)	0.636(93)
$C_{1123}^{LQ}, C_{1123}^{Ld})$	0.844(59)	0.807(41)	0.679(84)	$-0.457(59)$	$-0.548(77)$	0.784(57)	0.629(93)	0.681(84)	0.791(56)	0.630(93)
$(C_{2311}^{Qe}, C_{1123}^{ed})$	0.857(62)	0.816(44)	0.692(92)	$-0.468(60)$	$-0.558(77)$	0.81(35)	0.67(12)	0.690(94)	0.82(37)	0.66(12)
$(C_{2311}^{Qe}, C_{1123}^{Ld})$	0.856(59)	0.825(41)	0.716(87)	$-0.481(59)$	$-0.578(76)$	0.590(75)	0.77(10)	0.729(87)	0.590(75)	0.76(10)
$(C_{2223}^{LQ}, C_{2322}^{Qe}, C_{1123}^{LQ}, C_{2311}^{Qe})$	0.806(56)	0.845(29)	0.743(69)	$-0.477(63)$	$-0.584(83)$	0.71(16)	0.768(61)	0.744(70)	0.71(17)	0.765(62)
	0.805(55)	*0.849(26)*	*0.763(59)*	*$-0.495(54)$*	*$-0.648(48)$*	*0.71(16)*	*0.795(54)*	*0.761(61)*	*0.72(16)*	*0.790(54)*
All	0.838(60)	0.792(48)	0.638(89)	$-0.475(65)$	$-0.558(83)$	0.66(32)	0.70(19)	0.641(90)	0.67(33)	0.70(19)
	0.838(60)	*0.793(49)*	*0.650(89)*	*$-0.508(57)$*	*$-0.660(53)$*	*0.60(28)*	*0.77(23)*	*0.642(90)*	*0.61(29)*	*0.75(21)*
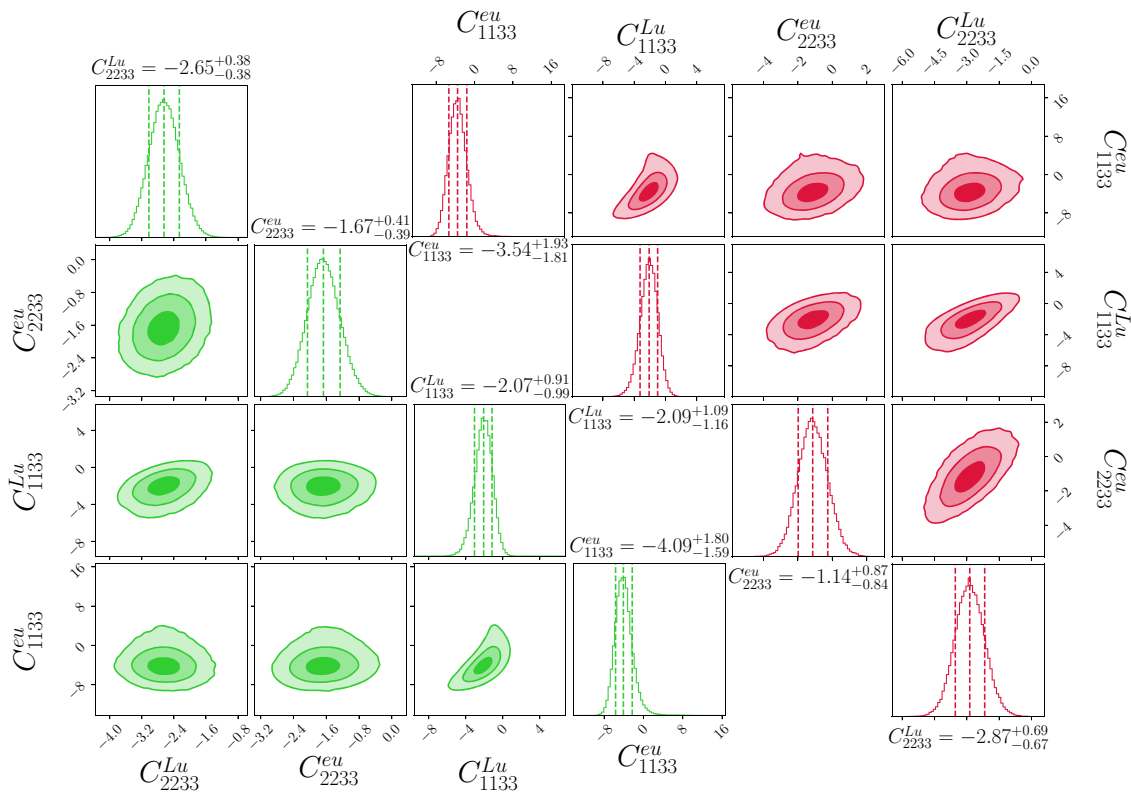
Fig. 10 Global fit of RGE-induced contributions ($\Lambda = 1$ *TeV*) from Eq. (17) constrained by $b \to s\ell^+\ell^-$ data within the PMD (green) and PDD (red) approach, including the new R_K measurement. 16-th, 50-th, 84-th percentile for marginalized distributions is shown
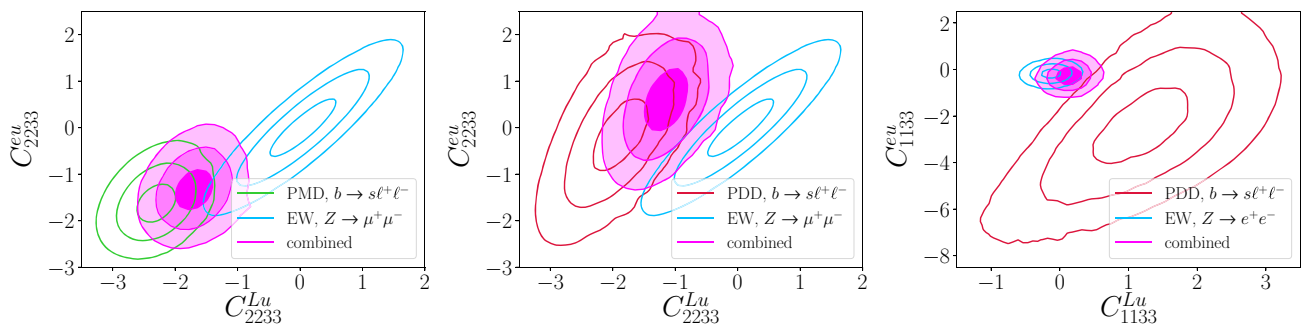

Fig. 11 2D p.d.f. for the scenario with WCs ($C^{Lu}_{\ell\ell33}, C^{eu}_{\ell\ell33}$) in both the PMD and the PDD approach, following the colour scheme defined below Fig. 2. EW constraints on these scenario from $Z \to \ell^+\ell^-$ mea-surements [207] are shown in light blue. The resulting region obtained from the combined information of EW and $b \to s\ell^+\ell^-$ data is high-lighted in fuchsia

too, and a minor role played by the two operators related to the electron mode. This outcome falls within the expectations of what has been repeatedly observed in the present study for the $B \to K^*\mu^+\mu^-$ angular analysis. In the PDD approach, the interplay between the two muonic operators redistribute the effects amongst the whole set of four operators in adjust-ment of possible large hadronic effects in the $B \to K^*\ell^+\ell^-$ amplitude. The WC of O^{Lu}_{2233} is well-determined at more than 4σ, the other ones are compatible with 0 within 2σ.

The overall goodness of the fit is exactly the same as for the case of the tree-level SMEFT scenario delineated by the set ($O^{LQ}_{2223,1123}, O^{Qe}_{2322,2311}$), inspected in Sect. 4. Identical con-siderations hold in particular for the observables presented in Table 4. Within the PDD approach, such scenario adequately describes the current dataset, as in the right panel of Fig. 4. On the other hand – if a more restrictive role needs to be assigned eventually to QCD power corrections – the LHCb update on R_K would actually disfavour this scenario in com-

parison with alternatives featuring NP effects in right-handed $b \to s$ currents too.

Eventually, as first studied in Ref. [224], and recently reviewed in light of $R_{K^{(*)}}$ anomalies in [131], the top-quark operators can be sensitive at the loop level to LEP-I measurements, mainly via the modification of the Z-boson decay rate and the corresponding left-right leptonic asymmetries. A convenient language in order to easily capture these modifications of Z-boson properties is given by the parameters $[\delta g_{L,R}^{Ze}]_{\ell^+\ell^-}$ scrutinized in Ref. [207]. In the leading-log approximation and at the leading order in the top Yukawa coupling, the contribution from $O_{\ell\ell 33}^{Lu,eu}$ via RGE is [203]:

$$[\delta g_L^{Ze}]_{\ell\ell} = 3 \left(\frac{y_t v}{4\pi \Lambda}\right)^2 \log\left(\Lambda/\mu_{EW}\right) C_{\ell\ell 33}^{Lu} ,$$
$$[\delta g_R^{Ze}]_{\ell\ell} = 3 \left(\frac{y_t v}{4\pi \Lambda}\right)^2 \log\left(\Lambda/\mu_{EW}\right) C_{\ell\ell 33}^{eu} . \qquad \text{(B.1)}$$

In Fig. 11 we show the constraints on the WCs of $O_{\ell\ell 33}^{Lu,eu}$ coming from EW data. We focus on the muon and electron sector separately, mapping what is given in equation (4.6) of Ref. [207], using the correlations given in Appendix B of their work and noting that the two sets $[\delta g_{L,R}^{Ze}]_{ee}$ and $[\delta g_{L,R}^{Ze}]_{\mu\mu}$ are weakly correlated. The resulting bounds are shown as 1,2,3σ contours in light blue in the $C_{\ell\ell 33}^{Lu}$–$C_{\ell\ell 33}^{eu}$ plane. They are obtained assuming $\Lambda = 1$ TeV and evaluated at a matching scale μ_{EW} close to the top-quark mass to possibly minimize the overall matching-scale dependence [76,193]. In the same figure, we also show the joint probability distribution obtained for the same WCs from the analysis of $b \to s\ell^+\ell^-$ data. As usual, we restrict the analysis of the electron mode to the PDD framework only, in virtue of the information arising from the $B \to K^*\mu\mu$ angular observables. Eventually, we also highlight in fuchsia the region obtained combining flavour data of interest with the aforementioned LEP-I results.

The outcome depicted in Fig. 11 is pretty informative. On the left and central panel, a mild tension stands out between the highest probability region controlled by the $Z \to \mu^+\mu^-$ data and the one identified by the global $b \to s\ell^+\ell^-$ analysis. As a result of the interplay between the two experimental handles, a very different outcome for NP is expected depending on the hadronic assumptions involved. In the PDD approach, one may end up looking for NP effects mainly in O_{2233}^{Lu}, with a minor role played by the operator O_{2233}^{eu} possibly identified by $C_{2233}^{eu} > 0$; in the PMD approach the presence of the latter is actually ensured by $C_{2233}^{eu} < 0$ at the 3σ level. Lastly, the right panel of Fig. 11 shows how LEP-I measurements strongly constrain such a possibility with top-quark operators.

To sum up, for $O_{\ell\ell 33}^{Lu,eu}$ and $b \to s\ell^+\ell^-$ anomalies the coupling to muons is allowed by EW data and remains interesting as long as the hint for NP effects in right-handed $b \to s$ currents – as a mild implication of the present R_K update –

will not be further corroborated by other new measurements. An important caveat here is that the assumption regarding the absence of tree-level contributions in the EW fit that may easily relax the $Z \to \ell^+\ell^-$ constraints. A more refined analysis on this aspect will be presented elsewhere.

References

1. J. Gratrex, M. Hopfer, R. Zwicky, Generalised helicity formalism, higher moments and the $B \to K_{J_K}(\to K\pi)\bar\ell_1\ell_2$ angular distributions. Phys. Rev. D **93**, 054008 (2016). arXiv:1506.03970
2. G. Hiller, F. Kruger, More model-independent analysis of $b \to s$ processes. Phys. Rev. D **69**, 074020 (2004). arXiv:hep-ph/0310219
3. C. Bobeth, G. Hiller, G. Piranishvili, Angular distributions of $\bar B \to \bar K\ell^+\ell^-$ decays. JHEP **12**, 040 (2007). arXiv:0709.4174
4. C. Bobeth, G. Hiller, G. Piranishvili, CP asymmetries in bar $B \to \bar K^*(\to \bar K\pi)\bar\ell\ell$ and Untagged $\bar B_s, B_s \to \phi(\to K^+K^-)\bar\ell\ell$ Decays at NLO. JHEP **0807**, 106 (2008). arXiv:0805.2525
5. U. Egede, T. Hurth, J. Matias, M. Ramon, W. Reece, New observables in the decay mode $\bar B_d \to \bar K^{*0}l^+l^-$. JHEP **0811**, 032 (2008). arXiv:0807.2589
6. J. Matias, F. Mescia, M. Ramon, J. Virto, Complete anatomy of $\bar B_d \to \bar K^{*0}(\to K\pi)l^+l^-$ and its angular distribution. JHEP **1204**, 104 (2012). arXiv:1202.4266
7. LHCB collaboration, R. Aaij et al., Measurement of form-factor-independent observables in the decay $B^0 \to K^{*0}\mu^+\mu^-$. Phys. Rev. Lett. **111**, 191801 (2013). arXiv:1308.1707
8. LHCB collaboration, R. Aaij et al., Differential branching fractions and isospin asymmetries of $B \to K^{(*)}\mu^+\mu^-$ decays. JHEP **06**, 133 (2014). arXiv:1403.8044
9. LHCB collaboration, R. Aaij et al., Angular analysis of charged and neutral $B \to K\mu^+\mu^-$ decays. JHEP **05**, 082 (2014). arXiv:1403.8045
10. LHCB collaboration, R. Aaij et al., Angular analysis of the $B^0 \to K^{*0}\mu^+\mu^-$ decay using 3 fb^{-1} of integrated luminosity. JHEP **02**, 104 (2016). arXiv:1512.04442
11. LHCB collaboration, R. Aaij et al., Angular analysis of the $B^0 \to K^{*0}$ e$^+$ e$^-$ decay in the low-q^2 region. JHEP **04**, 064 (2015). arXiv:1501.03038
12. LHCB collaboration, R. Aaij et al., Angular analysis and differential branching fraction of the decay $B_s^0 \to \phi\mu^+\mu^-$. JHEP **09**, 179 (2015). arXiv:1506.08777
13. LHCB collaboration, R. Aaij et al., Measurements of the S-wave fraction in $B^0 \to K^+\pi^-\mu^+\mu^-$ decays and the $B^0 \to K^*(892)^0\mu^+\mu^-$ differential branching fraction. JHEP **11**, 047 (2016). arXiv:1606.04731
14. BELLE collaboration, S. Wehle et al., Lepton-flavor-dependent angular analysis of $B \to K^*\ell^+\ell^-$. Phys. Rev. Lett. **118**, 111801 (2017). arXiv:1612.05014
15. ATLAS collaboration, M. Aaboud et al., Angular analysis of $B_d^0 \to K^*\mu^+\mu^-$ decays in pp collisions at $\sqrt{s} = 8$ TeV with the ATLAS detector. JHEP **10**, 047 (2018). arXiv:1805.04000
16. CMS collaboration, V. Khachatryan et al., Angular analysis of the decay $B^0 \to K^{*0}\mu^+\mu^-$ from pp collisions at $\sqrt{s} = 8$ TeV. Phys. Lett. B **753**, 424–448 (2016). arXiv:1507.08126
17. CMS collaboration, A.M. Sirunyan et al., Measurement of angular parameters from the decay $B^0 \to K^{*0}\mu^+\mu^-$ in proton–proton collisions at $\sqrt{s} = 8$ TeV. Phys. Lett. B **781**, 517–541 (2018). arXiv:1710.02846
18. CMS collaboration, A.M. Sirunyan et al., Angular analysis of the decay $B^+ \to K^+\mu^+\mu^-$ in proton–proton collisions at $\sqrt{s} = 8$ TeV. Phys. Rev. D **98** 112011, (2018). arXiv:1806.00636

19. C. Bobeth, G. Hiller, D. van Dyk, C. Wacker, The decay $B \rightarrow Kl^+l^-$ at low hadronic recoil and model-independent $\Delta B = 1$ constraints. JHEP **1201**, 107 (2012). arXiv:1111.2558

20. S. Descotes-Genon, J. Matias, M. Ramon, J. Virto, Implications from clean observables for the binned analysis of $B \rightarrow K^*\mu^+\mu^-$ at large recoil. JHEP **1301**, 048 (2013). arXiv:1207.2753

21. S. Descotes-Genon, T. Hurth, J. Matias, J. Virto, Optimizing the basis of $B \rightarrow K^*\ell^+\ell^-$ observables in the full kinematic range. JHEP **1305**, 137 (2013). arXiv:1303.5794

22. J. Matias, N. Serra, Symmetry relations between angular observables in $B^0 \rightarrow K^*\mu^+\mu^-$ and the LHCb P_5' anomaly. Phys. Rev. D **90**, 034002 (2014). arXiv:1402.6855

23. A. Khodjamirian, T. Mannel, A. Pivovarov, Y.-M. Wang, Charm-loop effect in $B \rightarrow K^{(*)}\ell^+\ell^-$ and $B \rightarrow K^*\gamma$. JHEP **1009**, 089 (2010). arXiv:1006.4945

24. A. Khodjamirian, T. Mannel, Y.M. Wang, $B \rightarrow K\ell^+\ell^-$ decay at large hadronic recoil. JHEP **02**, 010 (2013). arXiv:1211.0234

25. J. Lyon, R. Zwicky, Resonances gone topsy turvy—the charm of QCD or new physics in $b \rightarrow s\ell^+\ell^-$? arXiv:1406.0566

26. B. Capdevila, S. Descotes-Genon, L. Hofer, J. Matias, Hadronic uncertainties in $B \rightarrow K^* \mu^+ \mu^-$: a state-of-the-art analysis. JHEP **04**, 016 (2017). arXiv:1701.08672

27. T. Blake, U. Egede, P. Owen, K.A. Petridis, G. Pomery, An empirical model to determine the hadronic resonance contributions to $\overline{B}^0 \rightarrow \overline{K}^{*0}\mu^+\mu^-$ transitions. Eur. Phys. J. C **78**, 453 (2018). arXiv:1709.03921

28. C. Bobeth, M. Chrzaszcz, D. van Dyk, J. Virto, Long-distance effects in $B \rightarrow K^*\ell\ell$ from analyticity. Eur. Phys. J. C **78**, 451 (2018). arXiv:1707.07305

29. S. Jäger, J.M. Camalich, On $B \rightarrow Vll$ at small dilepton invariant mass, power corrections, and new physics. JHEP **1305**, 043 (2013). arXiv:1212.2263

30. S. Jäger, J.M. Camalich, Reassessing the discovery potential of the $B \rightarrow K^*\ell^+\ell^-$ decays in the large-recoil region: SM challenges and BSM opportunities. Phys. Rev. D **93**, 014028 (2016). arXiv:1412.3183

31. M. Ciuchini, M. Fedele, E. Franco, S. Mishima, A. Paul, L. Silvestrini et al., $B \rightarrow K^*\ell^+\ell^-$ decays at large recoil in the Standard Model: a theoretical reappraisal. JHEP **06**, 116 (2016). arXiv:1512.07157

32. M. Ciuchini, M. Fedele, E. Franco, S. Mishima, A. Paul, L. Silvestrini et al., $B \rightarrow K^*\ell^+\ell^-$ in the Standard Model: elaborations and interpretations. PoS **ICHEP2016**, 584 (2016). arXiv:1611.04338

33. M. Ciuchini, M. Fedele, E. Franco, S. Mishima, A. Paul, L. Silvestrini et al., Knowns and unknowns in the predictions for $B \rightarrow K^*\mu^+\mu^-$. Nucl. Part. Phys. Proc. **285–286**, 45–49 (2017)

34. BELLE II collaboration, W. Altmannshofer et al., *The Belle II Physics Book*. arXiv:1808.10567

35. B. Capdevila, S. Descotes-Genon, J. Matias, J. Virto, Assessing lepton-flavour non-universality from $B \rightarrow K^*\ell\ell$ angular analyses. JHEP **10**, 075 (2016). arXiv:1605.03156

36. N. Serra, R. Silva Coutinho, D. van Dyk, Measuring the breaking of lepton flavor universality in $B \rightarrow K^*\ell^+\ell^-$. Phys. Rev. D **95**, 035029 (2017). arXiv:1610.08761

37. J. Albrecht, F. Bernlochner, M. Kenzie, S. Reichert, D. Straub, A. Tully, Future prospects for exploring present day anomalies in flavour physics measurements with Belle II and LHCb. arXiv:1709.10308

38. A. Mauri, N. Serra, R.S. Coutinho, Towards establishing lepton flavor universality violation in $\bar{B} \rightarrow \bar{K}^*\ell^+\ell^-$ decays. Phys. Rev. D **99**, 013007 (2019). arXiv:1805.06401

39. M. Ciuchini, A.M. Coutinho, M. Fedele, E. Franco, A. Paul, L. Silvestrini et al., Hadronic uncertainties in semileptonic $B \rightarrow K^*\mu^+\mu^-$ decays. PoS **BEAUTY2018**, 044 (2018). arXiv:1809.03789

40. M. Bordone, G. Isidori, A. Pattori, On the Standard Model predictions for R_K and R_{K^*}. Eur. Phys. J. C **76**, 440 (2016). arXiv:1605.07633

41. LHCb collaboration, R. Aaij et al., Test of lepton universality using $B^+ \rightarrow K^+\ell^+\ell^-$ decays. Phys. Rev. Lett. **113**, 151601 (2014). arXiv:1406.6482

42. LHCb collaboration, R. Aaij et al., Test of lepton universality with $B^0 \rightarrow K^{*0}\ell^+\ell^-$ decays. JHEP **08**, 055 (2017). arXiv:1705.05802

43. R. Alonso, B. Grinstein, J. Martin Camalich, $SU(2) \times U(1)$ gauge invariance and the shape of new physics in rare B decays. Phys. Rev. Lett. **113**, 241802 (2014). arXiv:1407.7044

44. G. Hiller, M. Schmaltz, R_K and future $b \rightarrow s\ell\ell$ physics beyond the standard model opportunities. Phys. Rev. D **90**, 054014 (2014). arXiv:1408.1627

45. D. Ghosh, M. Nardecchia, S.A. Renner, Hint of lepton flavour non-universality in B meson decays. JHEP **12**, 131 (2014). arXiv:1408.4097

46. S.L. Glashow, D. Guadagnoli, K. Lane, Lepton flavor violation in B decays? Phys. Rev. Lett. **114**, 091801 (2015). arXiv:1411.0565

47. G. Hiller, M. Schmaltz, Diagnosing lepton-nonuniversality in $b \rightarrow s\ell\ell$. JHEP **02**, 055 (2015). arXiv:1411.4773

48. B. Gripaios, M. Nardecchia, S.A. Renner, Composite lepto-quarks and anomalies in B-meson decays. JHEP **05**, 006 (2015). arXiv:1412.1791

49. S. Sahoo, R. Mohanta, Scalar leptoquarks and the rare B meson decays. Phys. Rev. D **91**, 094019 (2015). arXiv:1501.05193

50. A. Crivellin, G. D'Ambrosio, J. Heeck, Addressing the LHC flavor anomalies with horizontal gauge symmetries. Phys. Rev. D **91**, 075006 (2015). arXiv:1503.03477

51. A. Crivellin, L. Hofer, J. Matias, U. Nierste, S. Pokorski, J. Rosiek, Lepton-flavour violating B decays in generic Z' models. Phys. Rev. D **92**, 054013 (2015). arXiv:1504.07928

52. A. Celis, J. Fuentes-Martin, M. Jung, H. Serodio, Family nonuniversal Z' models with protected flavor-changing interactions. Phys. Rev. D **92**, 015007 (2015). arXiv:1505.03079

53. R. Alonso, B. Grinstein, J. Martin Camalich, Lepton universality violation and lepton flavor conservation in B-meson decays. JHEP **10**, 184 (2015). arXiv:1505.05164

54. A. Greljo, G. Isidori, D. Marzocca, On the breaking of lepton flavor universality in B decays. JHEP **07**, 142 (2015). arXiv:1506.01705

55. L. Calibbi, A. Crivellin, T. Ota, Effective field theory approach to $b \rightarrow sll^{(')}$, $B \rightarrow K^{(*)}\nu\bar{\nu}$ and $B \rightarrow D^{(*)}\tau\nu$ with Third Generation Couplings. Phys. Rev. Lett. **115**, 181801 (2015). arXiv:1506.02661

56. A. Falkowski, M. Nardecchia, R. Ziegler, Lepton flavor non-universality in B-meson decays from a U(2) flavor model. JHEP **11**, 173 (2015). arXiv:1509.01249

57. A. Carmona, F. Goertz, Lepton flavor and nonuniversality from minimal composite higgs setups. Phys. Rev. Lett. **116**, 251801 (2016). arXiv:1510.07658

58. B. Allanach, F.S. Queiroz, A. Strumia, S. Sun, Z' models for the LHCb and $g-2$ muon anomalies. Phys. Rev. D **93**, 055045 (2016). arXiv:1511.07447

59. C.-W. Chiang, X.-G. He, G. Valencia, Z' model for $b \rightarrow s\ell\bar{\ell}$ flavor anomalies. Phys. Rev. D **93**, 074003 (2016). arXiv:1601.07328

60. D. Bečirević, O. Sumensari, R. Zukanovich Funchal, Lepton flavor violation in exclusive $b \rightarrow s$ decays. Eur. Phys. J. C **76**, 134 (2016). arXiv:1602.00881

61. F. Feruglio, P. Paradisi, A. Pattori, Revisiting lepton flavor universality in B decays. Phys. Rev. Lett. **118**, 011801 (2017). arXiv:1606.00524

62. E. Megias, G. Panico, O. Pujolas, M. Quiros, A natural origin for the LHCb anomalies. JHEP **09**, 118 (2016). arXiv:1608.02362

63. D. Bečirević, N. Košnik, O. Sumensari, R. Zukanovich Funchal, Palatable leptoquark scenarios for lepton flavor violation in exclusive $b \to s\ell_1\ell_2$ modes. JHEP **11**, 035 (2016). arXiv:1608.07583

64. P. Arnan, L. Hofer, F. Mescia, A. Crivellin, Loop effects of heavy new scalars and fermions in $b \to s\mu^+\mu^-$. JHEP **04**, 043 (2017). arXiv:1608.07832

65. W. Altmannshofer, S. Gori, S. Profumo, F.S. Queiroz, Explaining dark matter and B decay anomalies with an $L_\mu - L_\tau$ model. JHEP **12**, 106 (2016). arXiv:1609.04026

66. S. Sahoo, R. Mohanta, A.K. Giri, Explaining the R_K and $R_{D^{(*)}}$ anomalies with vector leptoquarks. Phys. Rev. D **95**, 035027 (2017). arXiv:1609.04367

67. R. Alonso, E. Fernandez Martinez, M.B. Gavela, B. Grinstein, L. Merlo, P. Quilez, Gauged lepton flavour. JHEP **12**, 119 (2016). arXiv:1609.05902

68. G. Hiller, D. Loose, K. Schonwald, Leptoquark flavor patterns and B decay anomalies. JHEP **12**, 027 (2016). arXiv:1609.08895

69. I. Galon, A. Kwa, P. Tanedo, Lepton-flavor violating mediators. JHEP **03**, 064 (2017). arXiv:1610.08060

70. A. Crivellin, J. Fuentes-Martin, A. Greljo, G. Isidori, Lepton flavor non-universality in B decays from dynamical yukawas. Phys. Lett. B **766**, 77–85 (2017). arXiv:1611.02703

71. I. García García, LHCb anomalies from a natural perspective. JHEP **03**, 040 (2017). arXiv:1611.03507

72. P. Cox, A. Kusenko, O. Sumensari, T.T. Yanagida, SU(5) unification with TeV-scale leptoquarks. JHEP **03**, 035 (2017). arXiv:1612.03923

73. S. Jäger, M. Kirk, A. Lenz, K. Leslie, Charming new physics in rare B-decays and mixing? Phys. Rev. D **97**, 015021 (2018). arXiv:1701.09183

74. E. Megias, M. Quiros, L. Salas, Lepton-flavor universality violation in R_K and $R_{D^{(*)}}$ from warped space. JHEP **07**, 102 (2017). arXiv:1703.06019

75. A. Crivellin, D. Müller, T. Ota, Simultaneous explanation of $R(D^{(*)})$ and $b \to s\mu^+\mu^-$: the last scalar leptoquarks standing. JHEP **09**, 040 (2017). arXiv:1703.09226

76. A. Celis, J. Fuentes-Martin, A. Vicente, J. Virto, Gauge-invariant implications of the LHCb measurements on lepton-flavor nonuniversality. Phys. Rev. D **96**, 035026 (2017). arXiv:1704.05672

77. D. Bečirević, O. Sumensari, A leptoquark model to accommodate $R_K^{\text{exp}} < R_K^{\text{SM}}$ and $R_{K^*}^{\text{exp}} < R_{K^*}^{\text{SM}}$. JHEP **08**, 104 (2017). arXiv:1704.05835

78. Y. Cai, J. Gargalionis, M.A. Schmidt, R.R. Volkas, Reconsidering the one leptoquark solution: flavor anomalies and neutrino mass. JHEP **10**, 047 (2017). arXiv:1704.05849

79. J.F. Kamenik, Y. Soreq, J. Zupan, Lepton flavor universality violation without new sources of quark flavor violation. Phys. Rev. D **97**, 035002 (2018). arXiv:1704.06005

80. F. Sala, D.M. Straub, A new light particle in B decays? Phys. Lett. B **774**, 205–209 (2017). arXiv:1704.06188

81. S. Di Chiara, A. Fowlie, S. Fraser, C. Marzo, L. Marzola, M. Raidal et al., Minimal flavor-changing Z' models and muon $g - 2$ after the R_{K^*} measurement. Nucl. Phys. B **923**, 245–257 (2017). arXiv:1704.06200

82. D. Ghosh, Explaining the R_K and R_{K^*} anomalies. Eur. Phys. J. C **77**, 694 (2017). arXiv:1704.06240

83. R. Alonso, P. Cox, C. Han, T.T. Yanagida, Anomaly-free local horizontal symmetry and anomaly-full rare B-decays. Phys. Rev. D **96**, 071701 (2017). arXiv:1704.08158

84. A. Greljo, D. Marzocca, High-p_T dilepton tails and flavor physics. Eur. Phys. J. C **77**, 548 (2017). arXiv:1704.09015

85. C. Bonilla, T. Modak, R. Srivastava, J.W.F. Valle, $U(1)_{B_3-3L_\mu}$ gauge symmetry as a simple description of $b \to s$ anomalies. Phys. Rev. D **98**, 095002 (2018). arXiv:1705.00915

86. F. Feruglio, P. Paradisi, A. Pattori, On the importance of electroweak corrections for B anomalies. JHEP **09**, 061 (2017). arXiv:1705.00929

87. J. Ellis, M. Fairbairn, P. Tunney, Anomaly-free models for flavour anomalies. Eur. Phys. J. C **78**, 238 (2018). arXiv:1705.03447

88. F. Bishara, U. Haisch, P.F. Monni, Regarding light resonance interpretations of the B decay anomalies. Phys. Rev. D **96**, 055002 (2017). arXiv:1705.03465

89. R. Alonso, P. Cox, C. Han, T.T. Yanagida, Flavoured $B - L$ local symmetry and anomalous rare B decays. Phys. Lett. B **774**, 643–648 (2017). arXiv:1705.03858

90. Y. Tang, Y.-L. Wu, Flavor non-universal gauge interactions and anomalies in B-meson decays. Chin. Phys. C **42**, 033104 (2018). arXiv:1705.05643

91. A. Datta, J. Kumar, J. Liao, D. Marfatia, New light mediators for the R_K and R_{K^*} puzzles. Phys. Rev. D **97**, 115038 (2018). arXiv:1705.08423

92. D. Das, C. Hati, G. Kumar, N. Mahajan, Scrutinizing R-parity violating interactions in light of $R_{K^{(*)}}$ data. Phys. Rev. D **96**, 095033 (2017). arXiv:1705.09188

93. D.N. Dinh, L. Merlo, S.T. Petcov, R. Vega-Álvarez, Revisiting minimal lepton flavour violation in the light of leptonic CP violation. JHEP **07**, 089 (2017). arXiv:1705.09284

94. D. Bardhan, P. Byakti, D. Ghosh, Role of tensor operators in R_K and R_{K^*}. Phys. Lett. B **773**, 505–512 (2017). arXiv:1705.09305

95. L. Di Luzio, M. Nardecchia, What is the scale of new physics behind the B-flavour anomalies? Eur. Phys. J. C **77**, 536 (2017). arXiv:1706.01868

96. C.-W. Chiang, X.-G. He, J. Tandean, X.-B. Yuan, $R_{K^{(*)}}$ and related $b \to s\ell\bar{\ell}$ anomalies in minimal flavor violation framework with Z' boson. Phys. Rev. D **96**, 115022 (2017). arXiv:1706.02696

97. B. Chauhan, B. Kindra, A. Narang, Discrepancies in simultaneous explanation of flavor anomalies and IceCube PeV events using leptoquarks. Phys. Rev. D **97**, 095007 (2018). arXiv:1706.04598

98. S.F. King, Flavourful Z' models for $R_{K^{(*)}}$. JHEP **08**, 019 (2017). arXiv:1706.06100

99. R.S. Chivukula, J. Isaacson, K.A. Mohan, D. Sengupta, E.H. Simmons, R_K anomalies and simplified limits on Z' models at the LHC. Phys. Rev. D **96**, 075012 (2017). arXiv:1706.06575

100. I. Doršner, S. Fajfer, D.A. Faroughy, N. Košnik, The role of the S_3 GUT leptoquark in flavor universality and collider searches. JHEP **10**, 188 (2017). arXiv:1706.07779

101. D. Buttazzo, A. Greljo, G. Isidori, D. Marzocca, B-physics anomalies: a guide to combined explanations. JHEP **11**, 044 (2017). arXiv:1706.07808

102. D. Choudhury, A. Kundu, R. Mandal, R. Sinha, Minimal unified resolution to $R_{K^{(*)}}$ and $R(D^{(*)})$ anomalies with lepton mixing. Phys. Rev. Lett. **119**, 151801 (2017). arXiv:1706.08437

103. J.M. Cline, J. Martin Camalich, B decay anomalies from non-abelian local horizontal symmetry. Phys. Rev. D **96**, 055036 (2017). arXiv:1706.08510

104. A. Crivellin, D. Müller, A. Signer, Y. Ulrich, Correlating lepton flavor universality violation in B decays with $\mu \to e\gamma$ using leptoquarks. Phys. Rev. D **97**, 015019 (2018). arXiv:1706.08511

105. S.-Y. Guo, Z.-L. Han, B. Li, Y. Liao, X.-D. Ma, Interpreting the $R_{K^{(*)}}$ anomaly in the colored Zee–Babu model. Nucl. Phys. B **928**, 435–447 (2018). arXiv:1707.00522

106. C.-H. Chen, T. Nomura, Penguin $b \to s\ell'^+\ell'^-$ and B-meson anomalies in a gauged $L_\mu - L_\tau$. Phys. Lett. B **777**, 420–427 (2018). arXiv:1707.03249

107. S. Baek, Dark matter contribution to $b \to s\mu^+\mu^-$ anomaly in local $U(1)_{L_\mu - L_\tau}$ model. Phys. Lett. B **781**, 376–382 (2018). arXiv:1707.04573

108. L. Bian, S.-M. Choi, Y.-J. Kang, H.M. Lee, A minimal flavored $U(1)'$ for B-meson anomalies. Phys. Rev. D **96**, 075038 (2017). arXiv:1707.04811

109. E. Megias, M. Quiros, L. Salas, Lepton-flavor universality limits in warped space. Phys. Rev. D **96**, 075030 (2017). arXiv:1707.08014

110. H.M. Lee, Gauged $U(1)$ clockwork theory. Phys. Lett. B **778**, 79–87 (2018). arXiv:1708.03564

111. N. Assad, B. Fornal, B. Grinstein, Baryon number and lepton universality violation in leptoquark and diquark models. Phys. Lett. B **777**, 324–331 (2018). arXiv:1708.06350

112. L. Di Luzio, A. Greljo, M. Nardecchia, Gauge leptoquark as the origin of B-physics anomalies. Phys. Rev. D **96**, 115011 (2017). arXiv:1708.08450

113. L. Calibbi, A. Crivellin, T. Li, Model of vector leptoquarks in view of the B-physics anomalies. Phys. Rev. D **98**, 115002 (2018). arXiv:1709.00692

114. J.M. Cline, B decay anomalies and dark matter from vectorlike confinement. Phys. Rev. D **97**, 015013 (2018). arXiv:1710.02140

115. M. Crispim Romao, S.F. King, G.K. Leontaris, Non-universal Z' from fluxed GUTs. Phys. Lett. B **782**, 353–361 (2018). arXiv:1710.02349

116. S. Descotes-Genon, M. Moscati, G. Ricciardi, Nonminimal 331 model for lepton flavor universality violation in $b \rightarrow s \ell \ell$ decays. Phys. Rev. D **98**, 115030 (2018). arXiv:1711.03101

117. W. Altmannshofer, M.J. Baker, S. Gori, R. Harnik, M. Pospelov, E. Stamou et al., Light resonances and the low-q² bin of R_{K^*}. JHEP **03**, 188 (2018). arXiv:1711.07494

118. L. Bian, H.M. Lee, C.B. Park, B-meson anomalies and Higgs physics in flavored $U(1)'$ model. Eur. Phys. J. C **78**, 306 (2018). arXiv:1711.08930

119. J.M. Cline, J.M. Cornell, $R(K^{(*)})$ from dark matter exchange. Phys. Lett. B **782**, 232–237 (2018). arXiv:1711.10770

120. F.J. Botella, G.C. Branco, M. Nebot, Singlet heavy fermions as the origin of B anomalies in flavour changing neutral currents. arXiv:1712.04470

121. L. Di Luzio, M. Kirk, A. Lenz, Updated B_s-mixing constraints on new physics models for $b \rightarrow s \ell^+ \ell^-$ anomalies. Phys. Rev. D **97**, 095035 (2018). arXiv:1712.06572

122. R. Barbieri, A. Tesi, B-decay anomalies in Pati–Salam SU(4). Eur. Phys. J. C **78**, 193 (2018). arXiv:1712.06844

123. F. Sannino, P. Stangl, D.M. Straub, A.E. Thomsen, Flavor physics and flavor anomalies in minimal fundamental partial compositeness. Phys. Rev. D **97**, 115046 (2018). arXiv:1712.07646

124. G. D'Ambrosio, A.M. Iyer, Flavour issues in warped custodial models: B anomalies and rare K decays. Eur. Phys. J. C **78**, 448 (2018). arXiv:1712.08122

125. S. Raby, A. Trautner, Vectorlike chiral fourth family to explain muon anomalies. Phys. Rev. D **97**, 095006 (2018). arXiv:1712.09360

126. M. Blanke, A. Crivellin, B meson anomalies in a Pati–Salam model within the Randall–Sundrum background. Phys. Rev. Lett. **121**, 011801 (2018). arXiv:1801.07256

127. A. Falkowski, S.F. King, E. Perdomo, M. Pierre, Flavourful Z' portal for vector-like neutrino dark matter and $R_{K^{(*)}}$. JHEP **08**, 061 (2018). arXiv:1803.04430

128. G. Arcadi, T. Hugle, F.S. Queiroz, The dark $L_\mu - L_\tau$ rises via kinetic mixing. Phys. Lett. B **784**, 151–158 (2018). arXiv:1803.05723

129. A.E. Cárcamo Hernández, S.F. King, Muon anomalies and the $SU(5)$ Yukawa relations. arXiv:1803.07367

130. D. Marzocca, Addressing the B-physics anomalies in a fundamental composite Higgs model. JHEP **07**, 121 (2018). arXiv:1803.10972

131. J.E. Camargo-Molina, A. Celis, D.A. Faroughy, Anomalies in bottom from new physics in top. Phys. Lett. B **784**, 284–293 (2018). arXiv:1805.04917

132. M. Bordone, C. Cornella, J. Fuentes-Martín, G. Isidori, Low-energy signatures of the PS³ model: from B-physics anomalies to LFV. JHEP **10**, 148 (2018). arXiv:1805.09328

133. K. Earl, T. Grégoire, Contributions to $b \rightarrow s \ell \ell$ anomalies from R-parity violating interactions. JHEP **08**, 201 (2018). arXiv:1806.01343

134. S. Matsuzaki, K. Nishiwaki, K. Yamamoto, Simultaneous interpretation of K and B anomalies in terms of chiral-flavorful vectors. JHEP **11**, 164 (2018). arXiv:1806.02312

135. D. Bečirević, I. Doršner, S. Fajfer, N. Košnik, D.A. Faroughy, O. Sumensari, Scalar leptoquarks from grand unified theories to accommodate the B-physics anomalies. Phys. Rev. D **98**, 055003 (2018). arXiv:1806.05689

136. S. Baek, C. Yu, Dark matter for $b \rightarrow s \mu^+ \mu^-$ anomaly in a gauged $U(1)_X$ model. JHEP **11**, 054 (2018). arXiv:1806.05967

137. S.F. King, $R_{K^{(*)}}$ and the origin of Yukawa couplings. JHEP **09**, 069 (2018). arXiv:1806.06780

138. J. Kumar, D. London, R. Watanabe, Combined explanations of the $b \rightarrow s \mu^+ \mu^-$ and $b \rightarrow c \tau^- \bar{\nu}$ anomalies: a general model analysis. Phys. Rev. D **99**, 015007 (2019). arXiv:1806.07403

139. C. Hati, G. Kumar, J. Orloff, A.M. Teixeira, Reconciling B-meson decay anomalies with neutrino masses, dark matter and constraints from flavour violation. JHEP **11**, 011 (2018). arXiv:1806.10146

140. D. Guadagnoli, M. Reboud, O. Sumensari, A gauged horizontal $SU(2)$ symmetry and $R_{K^{(*)}}$. JHEP **11**, 163 (2018). arXiv:1807.03285

141. I. de Medeiros Varzielas, S.F. King, $R_{K^{(*)}}$ with leptoquarks and the origin of Yukawa couplings. JHEP **11**, 100 (2018). arXiv:1807.06023

142. S.-P. Li, X.-Q. Li, Y.-D. Yang, X. Zhang, $R_{D^{(*)}}$, $R_{K^{(*)}}$ and neutrino mass in the 2HDM-III with right-handed neutrinos. JHEP **09**, 149 (2018). arXiv:1807.08530

143. R. Alonso, A. Carmona, B.M. Dillon, J.F. Kamenik, J. Martin Camalich, J. Zupan, A clockwork solution to the flavor puzzle. JHEP **10**, 099 (2018). arXiv:1807.09792

144. A. Azatov, D. Barducci, D. Ghosh, D. Marzocca, L. Ubaldi, Combined explanations of B-physics anomalies: the sterile neutrino solution. JHEP **10**, 092 (2018). arXiv:1807.10745

145. L. Di Luzio, J. Fuentes-Martin, A. Greljo, M. Nardecchia, S. Renner, Maximal flavour violation: a Cabibbo mechanism for leptoquarks. JHEP **11**, 081 (2018). arXiv:1808.00942

146. G.H. Duan, X. Fan, M. Frank, C. Han, J.M. Yang, A minimal $U(1)'$ extension of MSSM in light of the B decay anomaly. Phys. Lett. B **789**, 54–58 (2019). arXiv:1808.04116

147. J. Heeck, D. Teresi, Pati-Salam explanations of the B-meson anomalies. JHEP **12**, 103 (2018). arXiv:1808.07492

148. A. Angelescu, D. Bečirević, D.A. Faroughy, O. Sumensari, Closing the window on single leptoquark solutions to the B-physics anomalies. JHEP **10**, 183 (2018). arXiv:1808.08179

149. B. Grinstein, S. Pokorski, G.G. Ross, Lepton non-universality in B decays and fermion mass structure. JHEP **12**, 079 (2018). arXiv:1809.01766

150. S. Singirala, S. Sahoo, R. Mohanta, Exploring dark matter, neutrino mass and $R_{K^{(*)},\phi}$ anomalies in $L_\mu - L_\tau$ model. Phys. Rev. D **99**, 035042 (2019). arXiv:1809.03213

151. S. Balaji, R. Foot, M.A. Schmidt, Chiral SU(4) explanation of the $b \rightarrow s$ anomalies. Phys. Rev. D **99**, 015029 (2019). arXiv:1809.07562

152. P. Rocha-Moran, A. Vicente, Lepton flavor violation in a Z' model for the $b \rightarrow s$ anomalies. Phys. Rev. D **99**, 035016 (2019). arXiv:1810.02135

153. A. Kamada, M. Yamada, T.T. Yanagida, Self-interacting dark matter with a vector mediator: kinetic mixing with the $U(1)_{(B-L)_3}$ gauge boson. JHEP **03**, 021 (2019). arXiv:1811.02567

154. B. Fornal, S.A. Gadam, B. Grinstein, Left-right SU(4) vector leptoquark model for flavor anomalies. arXiv:1812.01603

155. C.-Q. Geng, H. Okada, Resolving B-meson anomalies by flavor-dependent gauged symmetries $\prod_{i=1}^{3} U(1)_{B_i - L_i}$. arXiv:1812.07918

156. J. Kumar, D. London, New physics in $b \rightarrow se^+ e^-$? arXiv:1901.04516

157. S. Baek, Scalar dark matter behind $b \rightarrow s\mu\mu$ anomaly. arXiv:1901.04761

158. C. Marzo, L. Marzola, M. Raidal, Common explanation to the $R_{K^{(*)}}$, $R_{D^{(*)}}$ and ϵ'/ϵ anomalies in a 3HDM+ν_R and connections to neutrino physics. arXiv:1901.08290

159. D.G. Cerdeño, A. Cheek, P. Martín-Ramiro, J.M. Moreno, B anomalies and dark matter: a complex connection. arXiv:1902.01789

160. S. Bhattacharya, A. Biswas, Z. Calcuttawala, S.K. Patra, An in-depth analysis of $b \rightarrow c(s)$ semileptonic observables with possible $\mu - \tau$ mixing. arXiv:1902.02796

161. P. Ko, T. Nomura, C. Yu, $b \rightarrow s\mu^+\mu^-$ anomalies and related phenomenology in $U(1)_{B_3 - x_\mu L_\mu - x_\tau L_\tau}$ flavor gauge models. arXiv:1902.06107

162. G. D'Amico, M. Nardecchia, P. Panci, F. Sannino, A. Strumia, R. Torre et al., Flavour anomalies after the R_{K^*} measurement. JHEP **09**, 010 (2017). arXiv:1704.05438

163. L.-S. Geng, B. Grinstein, S. Jäger, J. Martin Camalich, X.-L. Ren, R.-X. Shi, Towards the discovery of new physics with lepton-universality ratios of $b \rightarrow s\ell\ell$ decays. Phys. Rev. D **96**, 093006 (2017). arXiv:1704.05446

164. B. Capdevila, A. Crivellin, S. Descotes-Genon, J. Matias, J. Virto, Patterns of new physics in $b \rightarrow s\ell^+\ell^-$ transitions in the light of recent data. JHEP **01**, 093 (2018). arXiv:1704.05340

165. W. Altmannshofer, P. Stangl, D.M. Straub, Interpreting hints for lepton flavor universality violation. Phys. Rev. D **96**, 055008 (2017). arXiv:1704.05435

166. M. Ciuchini, A.M. Coutinho, M. Fedele, E. Franco, A. Paul, L. Silvestrini et al., On flavourful easter eggs for new physics hunger and lepton flavour universality violation. Eur. Phys. J. C **77**, 688 (2017). arXiv:1704.05447

167. G. Hiller, I. Nisandzic, R_K and R_{K^*} beyond the standard model. Phys. Rev. D **96**, 035003 (2017). arXiv:1704.05444

168. LHCb collaboration, R. Aaij et al., Search for lepton-universality violation in $B^+ \rightarrow K^+\ell^+\ell^-$ decays. arXiv:1903.09252

169. Belle collaboration, A. Abdesselam et al., Test of lepton flavor universality in $B \rightarrow K^*\ell^+\ell^-$ decays at Belle. arXiv:1904.02440

170. K.G. Chetyrkin, M. Misiak, M. Munz, Weak radiative B meson decay beyond leading logarithms. Phys. Lett. B **400**, 206–219 (1997). arXiv:hep-ph/9612313

171. A.J. Buras, M. Munz, Effective Hamiltonian for $B \rightarrow X_s e^+ e^-$ beyond leading logarithms in the NDR and HV schemes. Phys. Rev. D **52**, 186–195 (1995). arXiv:hep-ph/9501281

172. C. Bobeth, M. Misiak, J. Urban, Photonic penguins at two loops and m(t) dependence of $BR[B \rightarrow X(s)l^+l^-]$. Nucl. Phys. B **574**, 291–330 (2000). arXiv:hep-ph/9910220

173. P. Gambino, U. Haisch, Complete electroweak matching for radiative B decays. JHEP **10**, 020 (2001). arXiv:hep-ph/0109058

174. M. Misiak, M. Steinhauser, Three loop matching of the dipole operators for b → s gamma and b → s g. Nucl. Phys. B **683**, 277–305 (2004). arXiv:hep-ph/0401041

175. C. Bobeth, P. Gambino, M. Gorbahn, U. Haisch, Complete NNLO QCD analysis of $\bar{B} \rightarrow X_s \ell^+\ell^-$ and higher order electroweak effects. JHEP **0404**, 071 (2004). arXiv:hep-ph/0312090

176. P. Gambino, M. Gorbahn, U. Haisch, Anomalous dimension matrix for radiative and rare semileptonic B decays up to three loops. Nucl. Phys. B **673**, 238–262 (2003). arXiv:hep-ph/0306079

177. T. Huber, E. Lunghi, M. Misiak, D. Wyler, Electromagnetic logarithms in $\bar{B} \rightarrow X_s \ell^+\ell^-$. Nucl. Phys. B **740**, 105–137 (2006). arXiv:hep-ph/0512066

178. A. Bharucha, D.M. Straub, R. Zwicky, $B \rightarrow V\ell^+\ell^-$ in the Standard Model from light-cone sum rules. JHEP **08**, 098 (2016). arXiv:1503.05534

179. W. Altmannshofer, D.M. Straub, New physics in $b \rightarrow s$ transitions after LHC run 1. Eur. Phys. J. C **75**, 382 (2015). arXiv:1411.3161

180. S. Descotes-Genon, L. Hofer, J. Matias, J. Virto, Global analysis of $b \rightarrow s\ell\ell$ anomalies. JHEP **06**, 092 (2016). arXiv:1510.04239

181. V.G. Chobanova, T. Hurth, F. Mahmoudi, D. Martinez Santos, S. Neshatpour, Large hadronic power corrections or new physics in the rare decay $B \rightarrow K^*\mu^+\mu^-$? JHEP **07**, 025 (2017). arXiv:1702.02234

182. A.K. Alok, B. Bhattacharya, A. Datta, D. Kumar, J. Kumar, D. London, New physics in $b \rightarrow s\mu^+\mu^-$ after the measurement of R_{K^*}. Phys. Rev. D **96**, 095009 (2017). arXiv:1704.07397

183. T. Hurth, F. Mahmoudi, D. Martinez Santos, S. Neshatpour, Lepton nonuniversality in exclusive $b \rightarrow s\ell\ell$ decays. Phys. Rev. D **96**, 095034 (2017). arXiv:1705.06274

184. A. Paul, D.M. Straub, Constraints on new physics from radiative B decays. JHEP **04**, 027 (2017). arXiv:1608.02556

185. M. Algueró, B. Capdevila, S. Descotes-Genon, P. Masjuan, J. Matias, Are we overlooking lepton flavour universal new physics in $b \rightarrow s\ell\ell$? arXiv:1809.08447

186. M. Algueró, B. Capdevila, S. Descotes-Genon, P. Masjuan, J. Matias, What R_K and Q_5 can tell us about new physics in $b \rightarrow s\ell\ell$ transitions? arXiv:1902.04900

187. A. Arbey, T. Hurth, F. Mahmoudi, S. Neshatpour, Hadronic and new physics contributions to $b \rightarrow s$ transitions. Phys. Rev. D **98**, 095027 (2018). arXiv:1806.02791

188. N. Gubernari, A. Kokulu, D. van Dyk, $B \rightarrow P$ and $B \rightarrow V$ form factors from B-meson light-cone sum rules beyond leading twist. JHEP **01**, 150 (2019). arXiv:1811.00983

189. R.R. Horgan, Z. Liu, S. Meinel, M. Wingate, Lattice QCD calculation of form factors describing the rare decays $B \rightarrow K^*\ell^+\ell^-$ and $B_s \rightarrow \phi\ell^+\ell^-$. Phys. Rev. D **89**, 094501 (2014). arXiv:1310.3722

190. M. Beneke, T. Feldmann, D. Seidel, Systematic approach to exclusive $B \rightarrow Vl^+l^-$, $V\gamma$ decays. Nucl. Phys. B **612**, 25–58 (2001). arXiv:hep-ph/0106067

191. A. Kozachuk, D. Melikhov, Revisiting nonfactorizable charm-loop effects in exclusive FCNC B-decays. Phys. Lett. B **786**, 378–381 (2018). arXiv:1805.05720

192. M. Beneke, G. Buchalla, M. Neubert, C. Sachrajda, Penguins with charm and quark–hadron duality. Eur. Phys. J. C **61**, 439–449 (2009). arXiv:0902.4446

193. C. Bobeth, A.J. Buras, A. Celis, M. Jung, Yukawa enhancement of Z-mediated new physics in $\Delta S = 2$ and $\Delta B = 2$ processes. JHEP **07**, 124 (2017). arXiv:1703.04753

194. W. Buchmuller, D. Wyler, Effective lagrangian analysis of new interactions and flavor conservation. Nucl. Phys. B **268**, 621–653 (1986)

195. B. Grzadkowski, M. Iskrzynski, M. Misiak, J. Rosiek, Dimension-six terms in the Standard Model Lagrangian. JHEP **10**, 085 (2010). arXiv:1008.4884

196. J. Aebischer, A. Crivellin, M. Fael, C. Greub, Matching of gauge invariant dimension-six operators for $b \rightarrow s$ and $b \rightarrow c$ transitions. JHEP **05**, 037 (2016). arXiv:1512.02830

197. L. Silvestrini, M. Valli, Model-independent Bounds on the Standard Model Effective Theory from Flavour Physics. arXiv:1812.10913

198. S. Descotes-Genon, A. Falkowski, M. Fedele, M. González-Alonso, J. Virto, The CKM parameters in the SMEFT. arXiv:1812.08163

199. J. de Blas, M. Ciuchini, E. Franco, S. Mishima, M. Pierini, L. Reina et al., Electroweak precision observables and Higgs-boson signal strengths in the Standard Model and beyond: present and future. JHEP **12**, 135 (2016). arXiv:1608.01509

200. J. Ellis, C.W. Murphy, V. Sanz, T. You, Updated global SMEFT Fit to Higgs, Diboson and electroweak data. JHEP **06**, 146 (2018). arXiv:1803.03252

201. A.J. Buras, J. Girrbach-Noe, C. Niehoff, D.M. Straub, $B \rightarrow K^{(*)}\nu\overline{\nu}$ decays in the Standard Model and beyond. JHEP **02**, 184 (2015). arXiv:1409.4557

202. BABAR collaboration, J.P. Lees et al., Search for $B \rightarrow K^{(*)}\nu\overline{\nu}$ and invisible quarkonium decays. Phys. Rev. D **87**, 112005 (2013). arXiv:1303.7465

203. E.E. Jenkins, A.V. Manohar, M. Trott, Renormalization group evolution of the Standard Model dimension six operators I: formalism and lambda dependence. JHEP **10**, 087 (2013). arXiv:1308.2627

204. E.E. Jenkins, A.V. Manohar, M. Trott, Renormalization group evolution of the Standard Model dimension six operators II: Yukawa dependence. JHEP **01**, 035 (2014). arXiv:1310.4838

205. T. Hurth, S. Renner, W. Shepherd, Matching for FCNC effects in the flavour-symmetric SMEFT. arXiv:1903.00500

206. J. Aebischer, J. Kumar, P. Stangl, D.M. Straub, A Global Likelihood for Precision Constraints and Flavour Anomalies. arXiv:1810.07698

207. A. Efrati, A. Falkowski, Y. Soreq, Electroweak constraints on flavorful effective theories. JHEP **07**, 018 (2015). arXiv:1503.07872

208. M. Bordone, D. Buttazzo, G. Isidori, J. Monnard, Probing lepton flavour universality with $K \rightarrow \pi\nu\bar{\nu}$ decays. Eur. Phys. J. C **77**, 618 (2017). arXiv:1705.10729

209. S. Descotes-Genon, J. Matias, J. Virto, Understanding the $B \rightarrow K^*\mu^+\mu^-$ anomaly. Phys. Rev. D **88**, 074002 (2013). arXiv:1307.5683

210. G. Hiller, R. Zwicky, (A)symmetries of weak decays at and near the kinematic endpoint. JHEP **03**, 042 (2014). arXiv:1312.1923

211. "Hepfit, a tool to combine indirect and direct constraints on high energy physics." http://hepfit.roma1.infn.it/

212. A. Caldwell, D. Kollar, K. Kroninger, BAT: the Bayesian analysis toolkit. Comput. Phys. Commun. **180**, 2197–2209 (2009). arXiv:0808.2552

213. A. Gelman, J. Hwang, A. Vehtari, Understanding predictive information criteria for Bayesian models, arXiv e-prints (2013). arXiv:1307.5928

214. T. Ando, Predictive bayesian model selection. Am. J. Math. Manag. Sci. **31**, 13–38 (2011)

215. R.E. Kass, A.E. Raftery, Bayes factors. J. Am. Stat. Assoc. **90**, 773–795 (1995)

216. LHCB collaboration, R. Aaij et al., Measurement of the $B_s^0 \rightarrow \mu^+\mu^-$ branching fraction and effective lifetime and search for $B^0 \rightarrow \mu^+\mu^-$ decays. Phys. Rev. Lett. **118**, 191801 (2017). arXiv:1703.05747

217. CMS collaboration, S. Chatrchyan et al., Measurement of the $B_{(s)} \rightarrow \mu^+\mu^-$ branching fraction and search for $B^0 \rightarrow \mu^+\mu^-$ with the CMS experiment. Phys. Rev. Lett. **111**, 101804 (2013). arXiv:1307.5025

218. ATLAS collaboration, M. Aaboud et al., Study of the rare decays of B_s^0 and B^0 mesons into muon pairs using data collected during 2015 and 2016 with the ATLAS detector, Submitted to: JHEP (2018). arXiv:1812.03017

219. HFLAV collaboration, Y. Amhis et al., Averages of b-hadron, c-hadron, and τ-lepton properties as of summer 2016, Eur. Phys. J. C **77**, 895 (2017). arXiv:1612.07233

220. LHCB collaboration, R. Aaij et al., Measurement of the ratio of branching fractions $BR(B_0 \rightarrow K^{\star 0}\gamma)/BR(B_{s0} \rightarrow \phi\gamma)$ and the direct CP asymmetry in $B_0 \rightarrow K^{\star 0}\gamma$. Nucl. Phys. B **867**, 1–18 (2013). arXiv:1209.0313

221. J.A. Bailey et al., $B \rightarrow Kl^+l^-$ decay form factors from three-flavor lattice QCD. Phys. Rev. D **93**, 025026 (2016). arXiv:1509.06235

222. G. D'Ambrosio, A.M. Iyer, F. Piccinini, A.D. Polosa, Confronting B anomalies with atomic physics. arXiv:1902.00893

223. M. Chrzaszcz, A. Mauri, N. Serra, R. Silva Coutinho, D. van Dyk, Prospects for disentangling long- and short-distance effects in the decays $B \rightarrow K^*\mu^+\mu^-$. arXiv:1805.06378

224. J. de Blas, M. Chala, J. Santiago, Renormalization group constraints on new top interactions from electroweak precision data. JHEP **09**, 189 (2015). arXiv:1507.00757